AMERICAN SOCIETY FOR MICROBIOLOGY | Molecular and Cellular Biology®

RESEARCH ARTICLE

Poly(C)-Binding Protein Pcbp2 Enables Differentiation of Definitive Erythropoiesis by Directing Functional Splicing of the Runx1 Transcript

Louis R. Ghanem,[a,b,d] Andrew Kromer,[d] Ian M. Silverman,[d] Xinjun Ji,[d] Matthew Gazzara,[d] Nhu Nguyen,[d] Gabrielle Aguilar,[a] Massimo Martinelli,[a,c] Yoseph Barash,[d] Stephen A. Liebhaber[d,e]

[a]Gastroenterology, Hepatology and Nutrition Division, The Children's Hospital of Philadelphia, Philadelphia, Pennsylvania, USA

[b]Department of Pediatrics, Perelman School of Medicine at the University of Pennsylvania, Philadelphia, Pennsylvania, USA

[c]Department of Translational Medical Science, Section of Pediatrics, University of Naples Federico II, Naples, Italy

[d]Department of Genetics, Perelman School of Medicine at the University of Pennsylvania, Philadelphia, Pennsylvania, USA

[e]Department of Medicine, Perelman School of Medicine at the University of Pennsylvania, Philadelphia, Pennsylvania, USA

ABSTRACT Formation of the mammalian hematopoietic system is under a complex set of developmental controls. Here, we report that mouse embryos lacking the KH domain poly(C) binding protein, Pcbp2, are selectively deficient in the definitive erythroid lineage. Compared to wild-type controls, transcript splicing analysis of the Pcbp2$^{-/-}$ embryonic liver reveals accentuated exclusion of an exon (exon 6) that encodes a highly conserved transcriptional control segment of the hematopoietic master regulator, Runx1. Embryos rendered homozygous for a Runx1 locus lacking this cassette exon (Runx1ΔE6) effectively phenocopy the loss of the definitive erythroid lineage in Pcbp2$^{-/-}$ embryos. These data support a model in which enhancement of Runx1 cassette exon 6 inclusion by Pcbp2 serves a critical role in development of hematopoietic progenitors and constitutes a critical step in the developmental pathway of the definitive erythropoietic lineage.

KEYWORDS RNA processing, alternative splicing, Pcbp2, Runx1, erythropoiesis, primitive erythropoiesis, definitive erythropoiesis, hematopoiesis, myeloid stem cells, posttranscriptional control mechanisms

The development of the mammalian erythroid system is a highly complex process involving successive lineage commitments and corresponding levels of molecular controls (1). Substantial efforts have gone into identifying various sets of transcription factors involved in these pathways and how they impact alterations in chromatin structures and PolII activities that drive erythroid lineage commitment. However, it is increasingly clear that the composition and function of the mRNAs that encode these factors can be significantly altered by layers of posttranscriptional controls. These controls are mediated by RNA-binding proteins as well as noncoding RNAs that impact mRNA processing, localization, translation, and turnover. Identifying the intersection of these transcriptional and posttranscriptional controls presents a critical challenge to achieving a comprehensive understanding of developmental pathways in general and in the specific pathways that drive the erythroid lineages.

Erythroid hematopoiesis is characterized by the generation of two successive lineages in the developing mouse embryo. Primitive erythroblasts derived from yolk sac blood islands first appear in the circulation at embryonic day 8.25 (E8.25) and can be

Received 11 April 2018 **Returned for modification** 10 May 2018 **Accepted** 26 May 2018

Accepted manuscript posted online 4 June 2018

Citation Ghanem LR, Kromer A, Silverman IM, Ji X, Gazzara M, Nguyen N, Aguilar G, Martinelli M, Barash Y, Liebhaber SA. 2018. Poly(C)-binding protein Pcbp2 enables differentiation of definitive erythropoiesis by directing functional splicing of the Runx1 transcript. Mol Cell Biol 38:e00175-18. https://doi.org/10.1128/MCB.00175-18.

Address correspondence to Louis R. Ghanem, ghaneml@email.chop.edu, or Stephen A. Liebhaber, liebhabe@mail.med.upenn.edu.

identified by their unique expression of the embryonic hemoglobin genes *Hbb-y* and *Hbb-bh1* (1, 2). Maturation of these primitive erythroblasts peaks between E9.0 and E12.0 (1, 3). A second wave of erythroid progenitors generates the definitive erythroid series. These cells derive primarily from the dorsal aorta and other embryonic vessels and seed the fetal liver and bone marrow beginning at E10.5 (4). The definitive erythroid cell lineage expresses the adult hemoglobin genes (*Hbb-bs*, *Hbb-bt*, *Hba-a1*, and *Hba-a2*) and represents the predominant red blood cell system that persists into adulthood (1, 4). The midgestational liver (E12.5 to E14.5) contains cells derived from both lineages, as they reciprocally change in their relative predominance, and is thus an optimal site for analysis of the lineage switching process. Importantly, the distinct spatial and temporal development of the primitive and definitive erythroid lineages suggests that unique developmental controls and regulatory circuits are required for their emergence.

Multiple studies have defined sets of transcription factors that mediate essential functions in erythroid lineage development (1, 5, 6). For example, Gata1 or Fog1 loss-of-function mutations block maturation of the primitive erythroid lineage at the proerythroblast stage and result in embryonic lethality at E9.5 to E10.5 (7). In contrast, development of the definitive erythroid lineage is markedly impaired in c-Myb and Klf1 null mice with midgestational lethality (8, 9). Expression of these and other transcription factors is under the control of additional upstream factors that serve as central drivers of hematopoietic commitment and erythroid lineage expansion and function. Prominent among the factors responsible for the most proximal decisions in erythroid lineage commitment is the transcription factor Runx1. Germ line inactivation of Runx1 in the mouse is embryonic lethal at E12.5, and the predominant impact of this inactivation on hematopoiesis is a selective and profound loss of the definitive erythroid lineage (10, 11).

While transcriptional factors such as Runx1 have been intensively studied for their contributions to erythroid lineage development, posttranscriptional controls in erythropoiesis have received less attention. A central role of posttranscriptional controls in erythropoiesis was initially described in the context of terminal erythrocyte maturation when transcription is being globally silenced and alterations in the transcriptome and protein expression are dependent on regulation of mRNA stability and translation (12–16). Analysis of these posttranscriptional controls have revealed important functions for a number of RNA binding proteins (RBPs). The roles of RBPs and posttranscriptional controls in modulating and driving the complex network of hematopoietic regulatory pathways remains to be more fully explored.

Poly(C) binding proteins (Pcbps; also referred to as hnRNPEs and αCPs) comprise a widely expressed and functionally heterogeneous gene family of RBPs (17–20). The Pcbps have specific relevance to normal erythroid differentiation and function. Studies have demonstrated that Pcbps support high levels of human adult α-globin mRNA expression by integrating nuclear and cytoplasmic events (21). These proteins were initially shown to stabilize cytoplasmic human α-globin mRNA and subsequently demonstrated to control transcript processing (splicing and cleavage/polyadenylation) in the nucleus of the erythroblast (16, 22–24). More recently we have demonstrated that Pcbp1 and Pcbp2 loci are independently essential for mouse embryonic viability, each impacting embryonic development at different stages (25). Pcbp1 null embryos lose viability very early (peri-implantation) in development, while Pcbp2 null embryos survive until midgestation (E12.5 to E13.5). Transcriptome analysis of Pcbp2 null fetal liver at E12.5 revealed substantial impairments in erythroblast maturation and megakaryocyte development that corresponded with global repression of transcriptional programs essential for these two hematopoietic lineages. These data suggest that Pcbp2 constitutes an important determinant of erythroid and megakaryocyte lineage development, most likely impacting the megakaryocyte-erythrocyte progenitor (MEP) cell population or their earlier myeloid stem cell progenitors (1, 26). While this impact of Pcbp2 on embryonic hematopoiesis has been demonstrated, the underlying mechanistic pathway(s) that is altered in Pcbp2 null embryos and the impact on posttran-

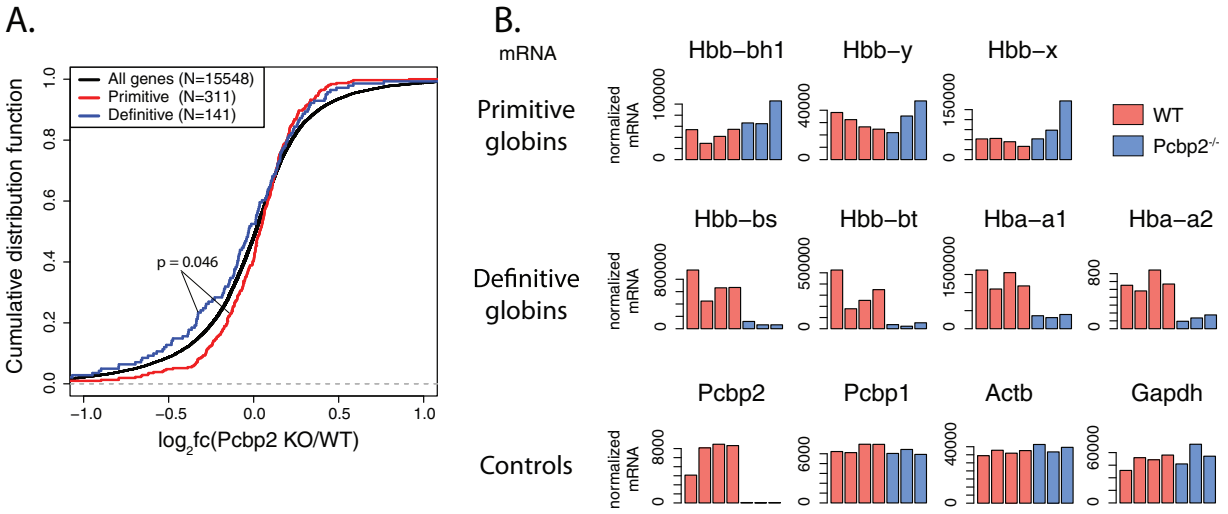

FIG 1 Development of the definitive erythroid lineage is selectively repressed in Pcbp2$^{-/-}$ fetal liver. (A) Cumulative distribution plot of gene expression changes (Pcbp2$^{-/-}$ versus WT, $\log_2$ fold change; GEO accession number GSE72491 [25]) for genes that characterize distinct erythroid lineages as defined by Greenfest-Allen et al. (N, total number of genes that define each lineage) (5). *P* values were determined using a Mann-Whitney U test. (B) Inactivation of the Pcbp2 loci (Pcbp2$^{-/-}$) impairs definitive globin gene expression. mRNA expression of primitive and definitive globin genes derived from RNA-seq data (25). Bars correspond to expression values derived from each biological replicate. Controls comprise four genes that are widely expressed in the mouse. The absence of Pcbp2 mRNA from the Pcbp2$^{-/-}$ sample confirms its gene deletion status.

scriptional controls relevant to hematopoietic lineage development and function remain undefined.

The current study describes the impact of Pcbp2 on the embryonic erythroid lineages and identifies an underlying molecular pathway. Analysis of midgestational embryos reveals that loss of Pcbp2 results in a pronounced and selective impairment of the definitive erythroid lineage while sparing the preceding primitive lineage. While no large shifts in steady-state levels of transcription factors linked to the definitive erythroid lineage were observed in the Pcbp2-null embryos that might account for this effect, a splicing analysis revealed that the loss of Pcbp2 resulted in a marked reduction in the inclusion of exon 6 in the Runx1 mRNA. This impact of Pcbp2 on Runx1 alternative splicing was linked to the presence of a high-affinity and evolutionarily conserved Pcbp2 binding site within the exon 6 splice acceptor (27). Analysis of embryos that were rendered homozygous for the Runx1ΔE6 mutation, resulting in loss of the exon 6-encoded protein segment, revealed a selective impairment of definitive erythroid lineage development that phenocopied that observed in Pcbp2-null mice. These data support a model where Pcbp2 drives development of the definitive erythroid lineage in the mouse embryo by enforcing retention of exon 6 in Runx1 mRNA. These findings establish a posttranscriptional control pathway that maintains the structure of a transcriptional factor critical to definitive erythropoiesis.

RESULTS

Pcbp2-null embryos (Pcbp2$^{-/-}$) have impaired development of the definitive erythroid lineage. Mouse embryos homozygous for germ line inactivation of the Pcbp2 locus (Pcbp2$^{-/-}$) lose viability at E13.5. Analysis of hematopoiesis in their livers at E12.5 reveals substantial defects in erythropoiesis, as reflected by a decrease in mature erythroblasts and reciprocal increase in erythroid progenitors (25). To further define this defect, we assessed the transcriptome signatures that distinguish the primitive and definitive erythroid lineages (1, 5). Transcriptome sequencing (RNA-seq) analysis of midgestational Pcbp2$^{-/-}$ embryos (E12.5) revealed a significant decrease in the expression of mRNAs that characterize the definitive lineage as opposed to primitive lineages (Fig. 1A) (*P* value of <0.05 by Mann-Whitney U test). These data pointed to a selective role of Pcbp2 in the generation of the definitive erythroid lineage in the mouse embryo.

Globin gene expression constitutes a landmark identifier of erythroid differentiation and delineates the primitive from definitive erythroid lineages. Embryonic globin genes are uniquely expressed in primitive erythroid cells, whereas adult globin genes are specific to definitive erythroid cells. Comparison of globin gene expression profiles from fetal livers of wild-type and Pcbp2$^{-/-}$ embryos revealed a selective and dramatic decrease in the expression of the definitive globin genes, while embryonic globin gene expression was fully maintained or slightly enhanced (Fig. 1B). Of note, expression of the major Pcbp paralog, Pcbp1, was unaffected in the Pcpb2$^{-/-}$ embryos. These data led us to conclude that Pcbp2 plays a nonredundant role in supporting the development of the definitive erythroid lineage in the embryonic mouse liver.

Splicing of the Runx1 transcript is markedly altered in Pcbp2$^{-/-}$ mice. Transcription factors linked to the differentiation of the primitive and definitive erythroid lineages have been well characterized (1, 5, 6). To account for the loss of definitive erythroid lineage development in the Pcpb2$^{-/-}$ embryos, we determined the extent to which select transcription factors that are upregulated during definitive erythroid differentiation (6) are impacted in Pcbp2$^{-/-}$ fetal livers. Surprisingly, this analysis failed to reveal any alterations greater than 2-fold in the steady-state levels of mRNAs encoding these erythroid cell-linked transcription factors (primitive erythroid cell specific, Pbx1, increased 30%, adjusted *P* value of 0.034 [values for Foxh1, Arid3a, Pdlim7, Cited2 were not significant]; definitive erythroid cell specific, Sox6 decreased 45%, adjusted *P* value of 0.004 [values for Nr3c1, Cebpa, Myb, and Irf9 were not significant]; GEO accession number GSE72491 [25]). Pcbp2 is a robust mediator of alternative splicing and previously has been shown to be responsible for the enhancement of splicing of a subset of cassette exons in mammalian erythroid cells (27). With this in mind, we mapped the splicing patterns of mRNAs in Pcbp2$^{-/-}$ embryos compared with those of wild-type controls. Fetal liver RNA-seq data sets (Pcbp2$^{-/-}$ versus wild type) previously established from E12.5 embryos (25) were compared using a robust pipeline for transcript structural analysis (modeling alternative junction inclusion quantification [MAJIQ] algorithm [28]). This analysis identified 76 high-confidence local splice variations (LSVs) within Pcbp2$^{-/-}$ fetal liver that contained one or more differentially spliced junctions in 64 genes (probability [|dPSI|, $\geq$20%], $>$95%) (see Table S3 in the supplemental material). One of the most strongly impacted splice junctions involved alternative splicing of exon 6 within the Runx1 transcript. There was a striking reduction in exon 6 inclusion in the Runx1 mRNA (Fig. 2A). The analysis failed to reveal significant alterations in the utilization of the other splice junctions in the Runx1 transcript or a change in steady-state Runx1 mRNA expression (Fig. 2B). This control of Runx1 exon 6 inclusion was of particular interest, as Runx1 is an extensively characterized and essential transcriptional regulator of embryonic hematopoiesis (10, 11) and exon 6 encodes a highly conserved and kinase-regulated determinant of Runx1 transcriptional activity (29–31). Importantly, there was no impact on splicing of any other Runx1 exons or on the corresponding exon in the transcript encoding the Runx1 paralog, Runx2 (Fig. 2C). These data are consistent with a model in which Pcbp2 enhances exon 6 inclusion in the Runx1 mRNA and suggest that this splicing control by Pcpb2 constitutes a critical step in the pathway of definitive erythropoiesis.

Concordant impacts of Pcbp$^{-/-}$ and Runx1$^{-/-}$ on hematopoietic gene expression in the embryonic liver. To further explore a potential linkage of Pcbp2 splicing control with Runx1 functions, we compared the effects of Pcbp2 loss (Pcbp$^{-/-}$) and of Runx1 loss (Runx1$^{-/-}$) on hematopoietic gene expression. The subset of genes that were compared were previously defined by chromatin immunoprecipitation sequencing (ChIP-seq) analysis as binding targets of Runx1 (32). This analysis revealed a remarkable concordance between the impacts of the two mouse knockout models (Fig. 3): Runx1 target genes whose expression positively correlated with the high Runx1 expression during endothelial-to-hematopoietic differentiation of embryonic stem cells had lower levels in Pcbp2$^{-/-}$ than wild-type fetal liver (*P* value of $<5.84 \times 10^{-5}$ by Mann-Whitney U test, correlated versus noncorrelated), while Runx1 target genes

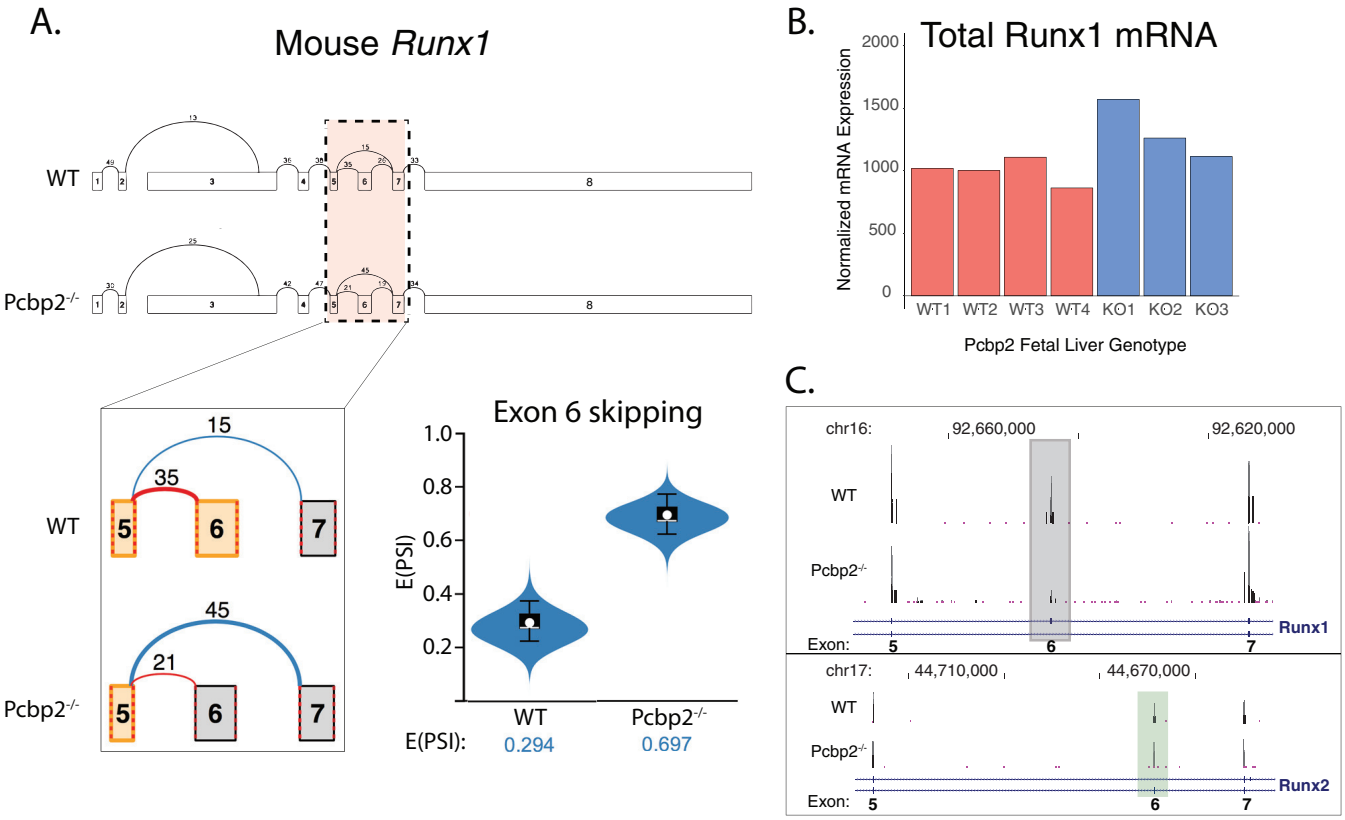

FIG 2 Splicing of Runx1 exon 6 is markedly repressed in Pcbp2$^{-/-}$ mice. (A) Impact of Pcbp2 on alternative splicing of the Runx1 transcript in the embryonic liver. The splice graph of the Runx1 transcript in wild-type (WT) and Pcbp$^{-/-}$ E12.5 fetal liver (defined by the MAJIQ builder and VOILA visualization tool [28]). Data were obtained from RNA-seq of WT and Pcbp2$^{-/-}$ embryonic liver (25). The numbers above each splice linkage represent the number of junction-spanning raw reads summed across all samples in that group. An expanded view of exon 6 alternative splicing is shown with exon 6 skipping represented by the blue line. The expected percent selected index, or E(PSI), for exon 6 skipping is summarized in the adjacent violin plot. E(PSI) is a statistical measure of each junction's inclusion or exclusion level in a given local splice variation (LSV) (see Materials and Methods). (B) Steady-state levels of Runx1 mRNA are unaltered in the Pcbp2$^{-/-}$ embryonic liver. Total steady-state Runx1 mRNA expression is taken from the RNA-seq data set and is shown in the histogram. Each bar corresponds to expression values derived from biological replicates with the noted genotypes. (C) Pcbp2 lacks significant impact on splicing of exon 6 in the Runx2 transcript. UCSC genome browser view of representative RNA-seq bar plots for murine Runx1 and Runx2 in WT and Pcbp2$^{-/-}$ fetal liver. Runx1 exon 6, black shading; Runx2 exon 6, green shading.

whose expression was higher when Runx1 expression was low (i.e., putatively suppressed by Runx1) had higher levels in the absence of Pcbp2 (P value of $<3.09 \times 10^{-5}$ by Mann-Whitney U test, correlated versus anticorrelated) (Fig. 3A). The expression of Runx1 target genes whose expression was unchanged in the comparison of wild-type and Runx1$^{-/-}$ samples was unchanged in Pcbp$^{-/-}$ fetal liver (not significant by Mann-Whitney U test) (Fig. 3A). Furthermore, genes either upregulated or downregulated in Runx1$^{-/-}$ vascular endothelial cadherin-positive embryonic cells at E7.5 were similarly altered in Pcbp2$^{-/-}$ fetal liver (P value of 2.44×10^{-10} by Mann-Whitney U test) (Fig. 3B). These data demonstrate that alterations of the hematopoietic transcriptome profile in Pcbp2$^{-/-}$ embryos are concordant with loss of Runx1 function and support a linkage between Pcbp2 and Runx1 functions that is mediated by the Pcbp2 enhancement of Runx1 exon 6 splicing.

Enhanced splicing of Runx1 exon 6 is linked to its conserved C-rich splice acceptor sequence and to the actions of Pcbp2. The importance of the exon 6-encoded protein segment to Runx1 function is supported by a high level of evolutionary conservation (Fig. 4A) and by its contribution to Runx1 transcriptional control functions (31). Pcbp2 is a KH domain RNA-binding protein with specific and high-affinity binding to C-rich motifs (33). Pcbp2 has been demonstrated to enhance cassette exon splicing by specific binding to polypyrimidine tract (PPT) splice acceptor sites that are enriched for C versus U content (27). The splice acceptor site of Runx1 exon 6 is

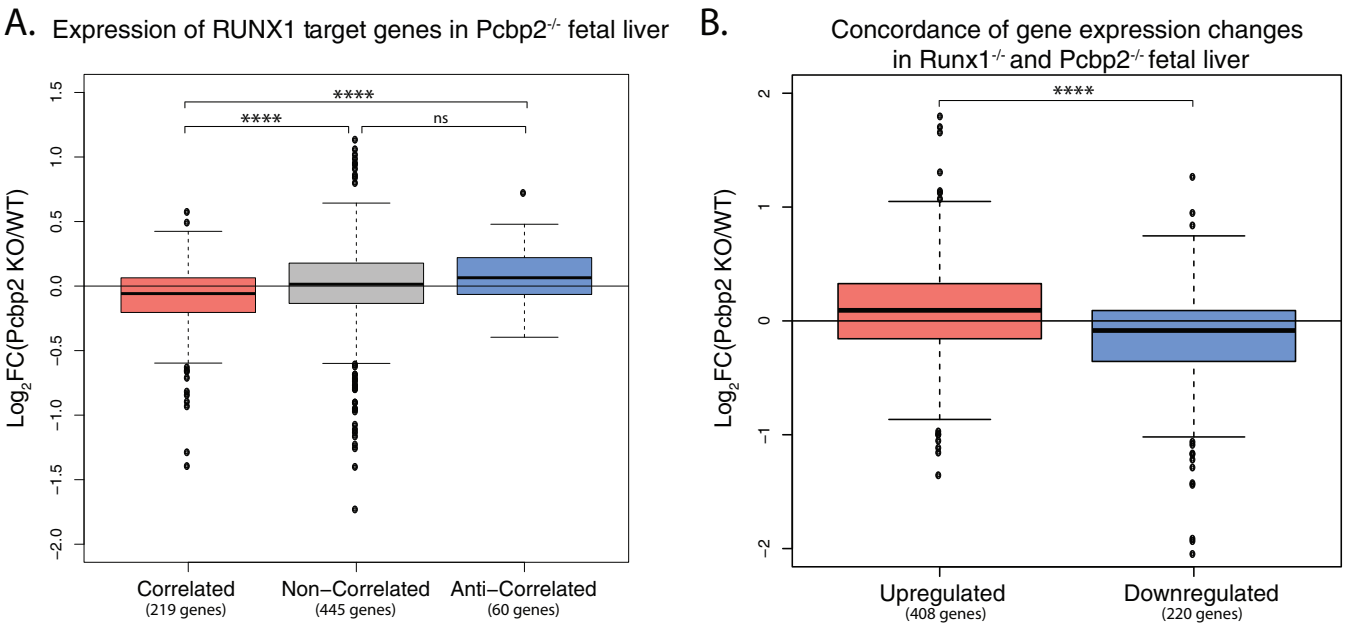

FIG 3 Positive correlation between the impacts of loss of Pcbp2 and Runx1 on the expression of Runx1 target genes. (A) Impact of Pcbp2 loss on the expression of Runx1 target genes demonstrates a significant alignment with the impacts of Runx1 itself. Comparison of direct Runx1 target genes from hematopoietic differentiation of embryonic stem cells described by Tanaka et al. and their relative expression changes in Pcbp2$^{-/-}$ fetal liver (32). Runx1 target genes were positively correlated ($n = 219$), noncorrelated ($n = 555$), and anticorrelated ($n = 65$) with Runx1 expression. (B) Comparison of genes impacted by Runx1 loss from VE-cadherin-positive E7.5 mouse embryo cells (32) and their relative expression changes in Pcbp2$^{-/-}$ fetal liver. Upregulated and downregulated denote gene sets with the corresponding expression change in Runx1$^{-/-}$ embryos.

remarkable for a C-rich PPT that is strongly conserved among mammalian species (Fig. 4B). This C-rich PPT structure contrasts with the canonical U-rich PPTs, bound by the U2AF65 splicing factor, that are found at the great majority of splice acceptor sites in mammalian genomes (34).

PPTs serve as a critical locus for splicing regulation. PPTs can be bound by multiple different RNA binding proteins that recognize a variety of pyrimidine-rich motifs and serve as platforms for multiple splice regulatory pathways (34). To further define the mechanistic basis for Pcbp2 control of exon 6 splicing, we selectively depleted K562, a human cancer cell line with some erythroblast characteristics, of each of 5 distinct and well-characterized PPT binding proteins associated with splicing controls: PCBP1, PCBP2, PTB, hnRNPK, and U2AF65. Each targeted depletion was verified by Western blotting (Fig. 4C), and the corresponding impact on RUNX1 exon 6 splicing was assayed by RT-PCR (Fig. 4D). Depletion of PCBP2 caused a substantial increase in exon 6 exclusion. Depletion of PCBP1 impacted exon 6 splicing in the same direction but was markedly less pronounced. Depletion of PTBP1 had no impact on exon 6 splicing, while depletions of hnRNPK and U2AF65 each triggered a decrease in exon 6 skipping (see Discussion). Thus, the impact of Pcbp2 on Runx1 exon 6 splicing that we observed in the embryonic mouse liver is conserved in human erythroblast cells. These data led us to conclude that Pcbp2 plays a specific and conserved role in the enhancement of exon 6 retention within Runx1 mRNA.

Generation of mice lacking exon 6 of Runx1 (Runx1ΔE6 allele). Runx1 and Pcbp2 are both essential gene products in the mouse, and Runx1$^{-/-}$ and Pcbp2$^{-/-}$ homozygous null embryos lose viability at approximately the same time in development (E12.5 to E13.5) (10, 11, 25). The concordant impairment of the definitive erythroid lineage in the midgestation livers of Runx1$^{-/-}$ (10, 11) and Pcbp2$^{-/-}$ embryos (25) further supported an overlap in their functions. The observation that Pcbp2 impacts the splicing of a conserved and functionally important exon (exon 6) of the Runx1 transcript suggested a mechanistic link between the actions of the Pcbp2 RNA-binding protein and the functions of the Runx1 transcription factor. The hypothesis that Runx1 exon 6 has a critical impact on the

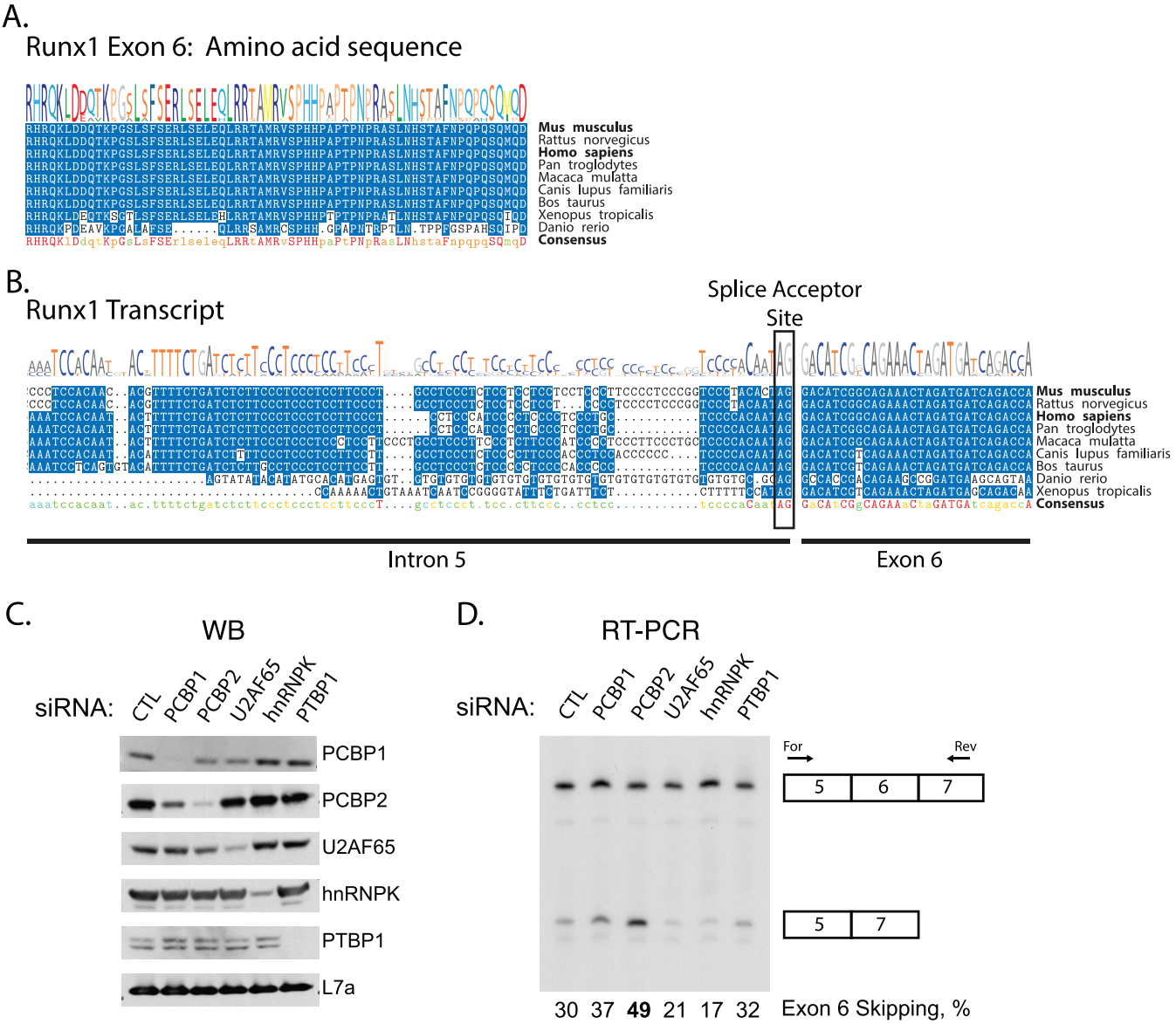

FIG 4 Conservation of Runx1 exon 6 coding potential, C-rich composition of its splice acceptor, and splicing enhancement by Pcbp2. (A) High-level conservation of the Runx1 exon 6-encoded protein segment. Comparison of Runx1 exon 6 amino acid sequences from the indicated vertebrate species. Proportional representation of the amino acids is displayed as a sequence logo above the alignment. Consensus amino acids are capitalized in red text beneath the alignment. Conserved amino acids are highlighted in blue. (B) A C-rich PPT is conserved 5′ to the Runx1 exon 6 splice acceptor. Exon 6 splice acceptor site and contiguous intron 5 sequences are displayed for the noted vertebrate species. The conserved C-rich PPT preceding the splice acceptor is highlighted in blue. Sequence logo and consensus are portrayed as described for panel A (alignment and image generated using ClustalW and the Multiple Sequence Alignment package [85]). (C) Specific depletion of five distinct polypyrimidine tract binding proteins from the human erythroblast cell line K562. Cells were depleted of each indicated protein by the corresponding siRNA. Western blot (WB) analysis confirms the effective protein depletions in each case. Ribosomal protein L7a serves as a loading control. (D) RUNX1 exon 6 skipping is selectively enhanced in Pcbp2-depleted cells. RT-PCR analysis of RUNX1 exon 6 skipping (amplification diagram to the right of the gel image) from siRNA-transfected cells as in panel C. Percentages of exon 6 skipping in each sample are shown. Arrows denote forward and reverse amplification primer positioning.

development of the definitive erythroid lineage was directly tested by assessing hematopoiesis in mice carrying a germ line deletion of exon 6 (Runx1ΔE6). Runx1ΔE6 mice were generated via a CRISPR-Cas9 gene-editing strategy (Fig. 5A). Germ line deletion of exon 6 was confirmed by sequencing across the targeted deletion junction (Fig. 5B). The impact of exon 6 deletion on Runx1 expression was assessed in midgestation fetal liver, a site of robust Runx1 expression and overlapping primitive and definitive erythropoietic lineages (35). Selective absence of exon 6 in Runx1 mRNA was confirmed in Runx1ΔE6 homozygous embryos by targeted RT-PCR (Fig. 5C). This loss of exon 6 had no significant impact on

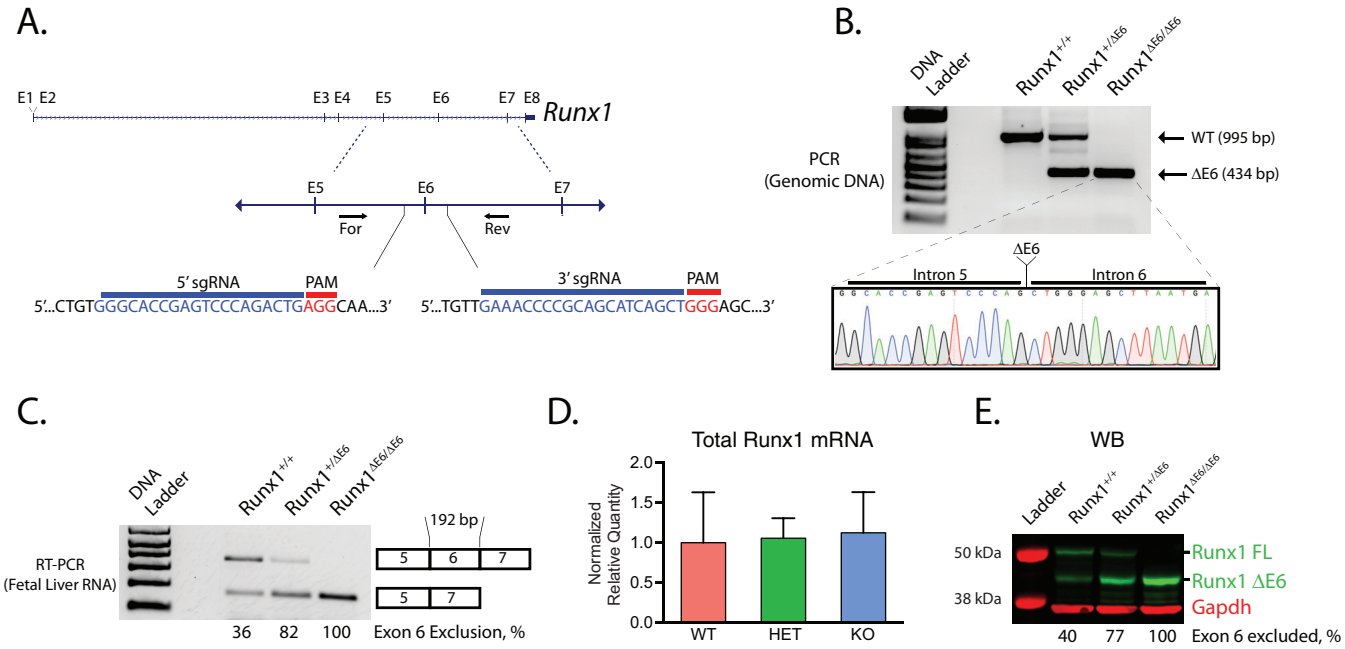

FIG 5 Generation of a Runx1 locus lacking exon 6 (Runx1ΔE6 allele) (A) Germ line deletion of mouse Runx1 exon 6 via CRISPR-Cas9-targeted cleavage. Schematic of the mouse Runx1 locus at exon 6 is shown with the guide RNA (sgRNA) target sequences indicated in blue and the protospacer adjacent motif (PAM) highlighted in red. Primer sites used for PCR genotyping are depicted (arrows). (B) Determinations of Runx1 exon 6 mutant allele genotypes. PCR analysis of the genomic region corresponding to exon 6 (primer positioning as described for panel A). Wild-type and mutant amplicon sizes are noted in the WT, heterozygote, and homozygote for the Runx1ΔE6 allele. The Sanger sequencing chromatogram confirms the exon 6 deletion junction of intron 5 and intron 6 in the mutant allele. (C) Runx1 mRNA transcript lacking exon 6 is generated from the Runx1ΔE6 allele. Total RNA from wild-type, Runx1ΔE6 heterozygous, and Runx1ΔE6 homozygous 14.5-dpc fetal livers were analyzed by RT-PCR across the exon 6 deletion site. The size of exon 6 and relative signal density (percentage) of the exon 6-deleted amplification product are indicated. (D) Wild-type levels of Runx1 mRNA are generated from the Runx1ΔE6 mutant allele. Total RNA from wild-type, Runx1ΔE6 heterozygous, and Runx1ΔE6 homozygous 14.5-dpc fetal liver were analyzed by qPCR for Runx1 mRNA expression. RT-PCR primers span exon 7 to exon 8 and capture all 4 annotated mouse splice variants. The standard errors for each sample are shown (minimum of three biological replicates per genotype). Statistical significance was determined by Student's *t* test. (E) Protein expressed from the Runx1$^{\Delta E6}$ mutant allele is of the predicted size for loss of exon 6 and is expressed at levels comparable to those of wild-type and heterozygous littermates. A representative Western blot from Runx1 wild-type, Runx1ΔE6 heterozygous, and Runx1ΔE6 homozygous fetal liver used in panels C and D is shown. Bands representing the full-length Runx1 isoform (FL) and the Runx1ΔE6 isoform are noted in green. Runx1 protein signal density was quantified and normalized to GAPDH expression. The relative signal density of the exon 6-deleted protein for each genotype is shown.

steady-state Runx1 mRNA levels (Fig. 5D), and Western blot analysis with a Runx1-specific antibody demonstrated a protein of the predicted apparent mass for Runx1ΔE6 (~45 to 47 kDa) (Fig. 5E). Total Runx1 protein levels (full length plus ΔE6 protein) demonstrated a 1.3-fold and 1.5-fold increase in Runx1$^{+/\Delta E6}$ and Runx1$^{\Delta E6/\Delta E6}$ mice, respectively, compared to levels of the wild type. Importantly, full-length Runx1 expression is entirely lost in Runx1$^{\Delta E6/\Delta E6}$ homozygous mice. These data confirm that the Runx1ΔE6 allele yields the predicted exon 6-deleted mRNA in the fetal liver and that a corresponding truncated Runx1 protein is generated without a substantial decrement in steady-state expression.

Viability of Runx1$^{\Delta E6/\Delta E6}$ embryos. The impact of the Runx1ΔE6 allele on organismal viability and growth was assessed by Runx1$^{\Delta E6/+}$ intercrosses. Analysis at E14.5 revealed a slight but significant decrease in viable Runx1$^{\Delta E6/\Delta E6}$ embryos compared to the expected Mendelian distribution (17% versus the expected 25.0%) (*P* value of 0.027; chi square, 7.237; degrees of freedom, 2) (Table 1). Genotyping at later stages (E15.5 through postnatal day 0 [P0]) revealed viable Runx1$^{\Delta E6/\Delta E6}$ progeny at frequencies comparable to those present at E14.5. Postnatal analysis of 7- to 10-day-old (P7 to P10) pups demonstrated a survival disadvantage of the Runx1$^{\Delta E6/\Delta E6}$ liveborns versus the wild type during weaning (Table 1). Male and female Runx1$^{\Delta E6/\Delta E6}$ mice that survived to adulthood were fertile and otherwise grossly normal. The viability of Runx1$^{\Delta E6/\Delta E6}$ mice through embryonic and into adult stages of life stands in sharp distinction to the uniform midgestational lethality observed in their germ line Runx1$^{-/-}$ counterparts (10, 11). The cause(s) of the reduced midgestational representation and diminished perinatal fitness of the Runx1$^{\Delta E6/\Delta E6}$ conceptions remains unexplored.

TABLE 1 Mice lacking Runx1 exon 6 are viable with reduced neonatal fitness[a]

	No. (%) of offspring resulting from $Runx1^{+/\Delta E6}$ × $Runx1^{+/\Delta E6}$ intercrosses			
Time point	Total	+/+	+/ΔE6	ΔE6/ΔE6
E14.5	165	62 (37.6)	75 (45.4)	28 (17.0)
E15.5–P0	58	14 (24.1)	32 (55.2)	12 (20.7)
7–14 days old	171	65 (38.2)	103 (60.6)	3 (1.8)

[a]Observed genotypes were from E14.5 embryos, those spanning E15.5 to postnatal day 0 (P0), and pups 1 to 2 weeks postpartum.

Maturation of the definitive erythroid series is impeded in the $Runx1^{\Delta E6/\Delta E6}$ fetal liver. Prior studies have demonstrated a failure of definitive erythroid development in midgestation $Runx1^{-/-}$ embryos with selective sparing of the primitive erythroid lineage (1, 10, 11). To determine if the Runx1ΔE6 mutation resulted in a similar impact on erythroid development, we examined erythroid maturation in E14.5 fetal livers, a developmental time point that fully captures late stages of definitive erythroid maturation. Mouse definitive erythroid differentiation from erythroid colony-forming cells (CFU-e; stage 0/1 [S0/S1]) to mature erythroblasts (S5) was stratified based upon the presence and expression levels of two validated erythroid cell surface markers, Ter119 and CD71 (36). These data revealed a significant delay in generation of the mature erythroblast populations (S4 and S5) and corresponding accumulation of immature cells (S1 and S2) in $Runx1^{\Delta E6/\Delta E6}$ fetal liver compared to wild-type and $Runx1^{+/\Delta E6}$ littermate controls (Fig. 6A and B). These data reveal that exon 6 of Runx1 serves a critical function in embryonic erythroid maturation.

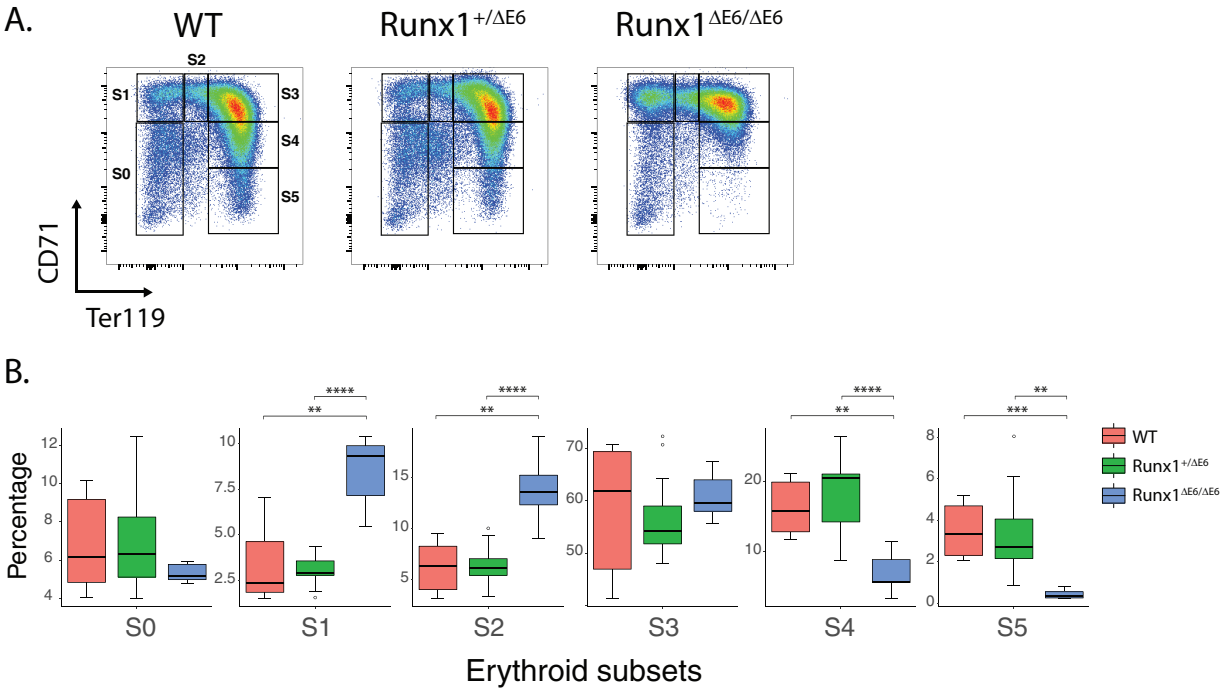

FIG 6 Erythroid differentiation is impaired in $Runx1^{\Delta E6/\Delta E6}$ fetal liver. (A) Flow cytometry of embryonic day 14.5 fetal liver reveals maturation arrest of definitive erythroid differentiation. Cells were harvested from Runx1 wild-type (WT), $Runx1^{+/\Delta E6}$, and $Runx1^{\Delta E6/\Delta E6}$ embryos and stained with antibodies to CD71 and Ter119. FACS images are representative of at least five biological replicates. There are 6 gating subsets that correspond to progressive stages of erythroblast differentiation (S0, progenitor; S5, mature erythroblast) (36). (B) Quantitative analysis of S0 to S5 erythroid subsets. Box plots of the data collected from the flow sorting analysis shown in panel A depict the median and 25th to 75th percentile range of total cell count percentages from each erythroid subset by genotype. Whiskers represent 1.5 times the interquartile range. Outliers beyond the whiskers are plotted individually. Statistical significance between groups was determined by 2-sided Student's *t* test (**, $P < 0.01$; ***, $P < 0.001$; ****, $P < 0.0001$).

Runx1 exon 6 deletion impairs hematopoietic progenitor function. Prior studies have revealed that Runx1 plays a critical role(s) at multiple stages of hematopoietic stem cell and myeloid lineage differentiation (10, 37). To determine if Runx1ΔE6 impacted specific myeloid progenitor populations, we assessed the relative abundance of fetal liver hematopoietic stem and myeloid progenitor cells by multiparameter flow cytometry of Lin^- $Sca1^+$ $c\text{-}Kit^+$ (LSK) cells (38). The fetal liver is normally enriched for long-term hematopoietic stem cells (HSCs) and progenitor cells capable of bone marrow reconstitution. The analysis of $Runx1^{\Delta E6/\Delta E6}$ fetal livers compared to wild-type and heterozygous controls revealed a significant loss in these precursor populations (Fig. 7A and B). Subset analysis of the LSK population revealed a significant decrease in multipotent progenitor (MPP) populations in Runx1ΔE6 heterozygous and homozygous fetal liver compared to the wild type and a corresponding increase in short-term HSCs. Myeloid progenitors from $Runx1^{\Delta E6/\Delta E6}$ fetal livers were significantly decreased for both the common myeloid progenitor (CMP) and granulocyte-monocyte progenitor (GMP) populations. These data point to an intrinsic defect in hematopoiesis in $Runx1^{\Delta E6/\Delta E6}$ fetal liver at the level of the hematopoietic stem cell or myeloid progenitor.

The functional capacity of fetal liver cells to undergo myeloid differentiation was further assessed using an *ex vivo* methylcellulose colony-forming assay (39). While no significant differences in colony-forming ability were observed between Runx1ΔE6 heterozygous and wild-type littermates (Fig. 7C), $Runx1^{\Delta E6/\Delta E6}$ embryos displayed a dramatic reduction in CFU-GM and CFU-E progenitors compared to controls. Of note, there was a virtual absence of early myeloid (CFU-GEMM) and early erythroid (BFU-E) progenitor colonies under these assay conditions. These data led us to conclude that Runx1 exon 6 function is required for hematopoietic progenitor cells to establish normal myeloid lineages in the fetal liver.

The selective loss of definitive globin gene expression in $Runx1^{\Delta E6/\Delta E6}$ embryonic liver phenocopies $Pcbp2^{-/-}$. To further define the impact of Runx1 exon 6 deletion on definitive erythroid development, we compared globin gene expression in wild-type, $Runx1^{+/\Delta E6}$, and $Runx1^{\Delta E6/\Delta E6}$ E12.5 fetal liver tissue. The analysis of $Runx1^{\Delta E6/\Delta E6}$ embryos revealed a significant decrease in adult globin expression in the Runx1ΔE6 embryos. This contrasted with robust expression of primitive hemoglobin gene expression (Fig. 7D). The selective depression of adult globin expression in the $Runx1^{\Delta E6/\Delta E6}$ embryos phenocopies $Pcbp2^{-/-}$ embryos (Fig. 1B). Runx1ΔE6 heterozygous embryos demonstrated intermediate levels of embryonic and adult globin gene expression compared to wild-type and $Runx1^{\Delta E6/\Delta E6}$ embryos. We conclude from these data that Runx1 exon 6 is critical for appropriately timed activation of definitive hemoglobin gene expression in mouse embryonic liver.

Hematopoietic defects in $Runx1^{\Delta E6/\Delta E6}$ adults. The observed defect in definitive erythropoiesis in the $Runx1^{\Delta E6/\Delta E6}$ E14.5 embryonic liver did not appear to significantly impact erythroid series steady-state levels in the adult. While $Runx1^{\Delta E6/\Delta E6}$ adults had minor changes in mean corpuscular volume (MCV) and mean corpuscular hemoglobin (MCH), the remainder of the red blood cell counts and indices were within normal limits (Fig. 8). Analysis of adult $Runx1^{\Delta E6/\Delta E6}$ animals did, however, reveal significant lymphopenia and thrombocytopenia, paralleling phenotypes previously reported in adult mice with conditional Runx1 knockout generated by interferon-inducible Mx-Cre-mediated recombination (37). While these data do not define the mechanism by which an essentially normal erythroid lineage is established in adult $Runx1^{\Delta E6/\Delta E6}$ mice despite the major alteration in definitive erythroid lineage development in the midgestation embryo, they are consistent with previously reported robust compensatory mechanisms in the murine hematopoietic system (40, 41).

DISCUSSION

Here, we explore the basis for impaired hematopoiesis in embryos lacking the RNA binding protein Pcbp2 ($Pcbp2^{-/-}$). We find that this defect is characterized by a selective repression of the definitive erythroid lineage (Fig. 1). The transcriptome of $Pcbp2^{-/-}$ embryos revealed a shift in alternative splicing of the Runx1 transcript with

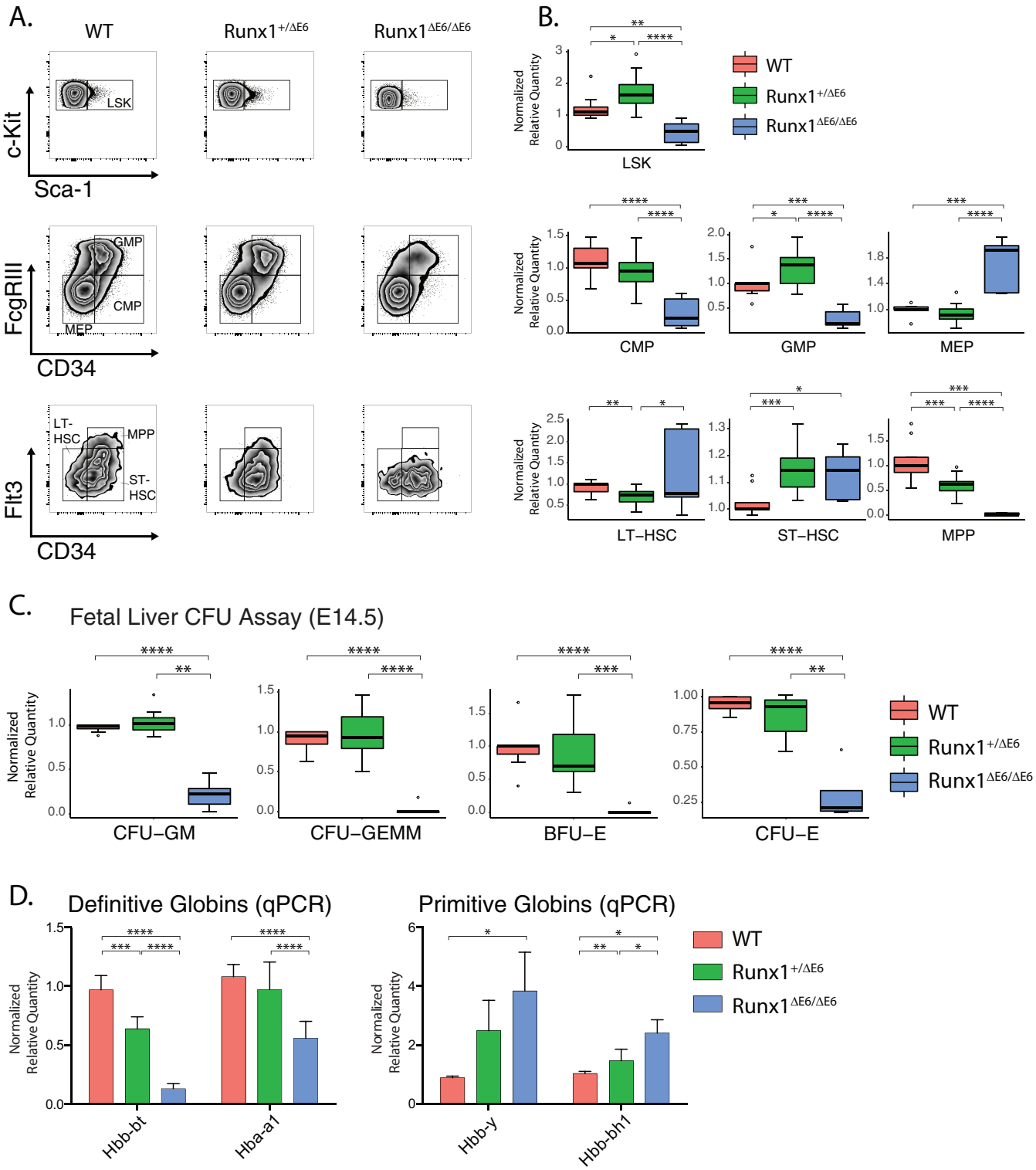

FIG 7 Runx1 exon 6 deletion impairs hematopoietic progenitor development and function. (A) Runx1 exon 6 is essential for normal production of hematopoietic multipotent progenitor (MPP) cells. Flow cytometry assay was performed on embryonic day 14.5 fetal liver cells from WT, Runx1$^{+/\Delta E6}$, and Runx1$^{\Delta E6/\Delta E6}$ embryos. FACS analysis of cells stained with the indicated hematopoietic stem cell and myeloid progenitor cell markers is depicted. (B) Quantitative analysis of hematopoietic progenitor populations. The data are derived from the flow analysis as presented in panel D. Box plots and statistical significance are as described for Fig. 6B. (C) Runx1 exon 6 function is required for myeloid progenitor differentiation. Hematopoietic progenitor colonies arising from *ex vivo* differentiation of E14.5 fetal liver embryonic stem cells. CFU-GM, CFU-GEMM, and BFU-E colonies were scored on day 7 of incubation, and CFU-E colonies were scored on day 2. A minimum of 6 embryos per genotype were analyzed across 4 litters. Colonies were counted per 1×10^4 fetal liver cells plated in triplicate. Data were normalized within litters, with the wild type set to 1. Box plots and statistical significance are as described for Fig. 6B. (D) Definitive hemoglobin mRNA expression is impaired in Runx1$^{\Delta E6/\Delta E6}$ fetal liver. Total RNA from WT, Runx1ΔE6 heterozygous, and Runx1ΔE6 homozygous 12.5-dpc fetal liver was analyzed

(Continued on next page)

a substantial reduction in cassette exon 6 retention (Fig. 2A). Runx1 (also referred to as AML1, CBFA2, and others) is a master transcriptional regulator of definitive hematopoiesis (42), and the segment of this protein encoded by exon 6 is highly conserved and is critical to Runx1 transcriptional function. We observed a significant correlation between the impacts of Pcbp2$^{-/-}$ and Runx1$^{-/-}$ genotypes on the expression of Runx1 target genes in hematopoietic and vascular tissues (Fig. 3) and on the development of the definitive hematopoietic lineage (10, 11). Based on these findings, we hypothesized that the defect in midgestational development of the definitive erythropoietic lineage in Pcbp2$^{-/-}$ embryos is mechanistically linked to the observed decrease in Runx1 exon 6 splicing. Exon 6 and its encoded protein segment are highly conserved in mammalian species (Fig. 4A and B) and critical to Runx1 function (29–31). Direct attribution of exon 6-encoded functions to definitive erythropoiesis was confirmed by analysis of embryos with germ line mutation of the Runx1 locus that eliminates exon 6 (Runx1$^{\Delta E6/\Delta E6}$) (Fig. 5). These studies serve to establish a mechanistic link between the actions of a specific RNA binding protein (Pcbp2) on cassette exon splicing with a subsequent impact on the function of a critical transcription factor (Runx1). This posttranscriptional pathway of gene regulation appears to play a pivotal role in hematopoietic development.

Runx1 expression is under a complex set of transcriptional and posttranscriptional controls. Runx1 isoforms are expressed from two distinct promoters in a tissue-dependent fashion (43–45). This results in expression of three major isoforms in humans (RUNX1a, RUNX1b, and RUNX1c) but only two in mice (Runx1b and Runx1c) (30). Exon 6 alternative splice variants from each of the major Runx1 isoforms have been described in human and mouse adult tissues and mouse fetal liver (46–48). Although the relative abundance of isoforms lacking exon 6 varies in a tissue-dependent manner (46), the major Runx1 isoforms in adult mouse bone marrow and fetal liver contain exon 6 (Fig. 5C) (30). The protein domain encoded by exon 6 resides between the DNA-binding domain (Runt homology domain) and C-terminal transactivation and autoinhibitory domains (44). Runx1 by itself is a weak transcriptional activator and most commonly heterodimerizes with core binding factor β or other transcription factors to activate or repress transcription (49, 50). Runx1 chromosomal inversions involving Runx1 account for ~20% of human acute myeloid leukemias. The most common of these, t(8;21), occurs at a chromosomal translocation hot spot in the human Runx1 locus between exon 5 and exon 6 and results in the AML1-ETO fusion oncoprotein which lacks exon 6 and all C-terminal functional domains (51). *In vitro* and cell line-based overexpression studies have demonstrated that Runx1 proteins lacking exon 6 have reduced transactivation potential (48, 52). Numerical and functional abnormalities in adult hematopoietic stem cells were recently reported to occur in a Runx1 mutant mouse that had constitutive exon 6 inclusion (30). These findings point to a functional role for alternative splicing of Runx1 exon 6 in developmental settings and imply that factors that control exon 6 inclusion are of importance to Runx1 function.

Our analysis of Pcbp2$^{-/-}$ fetal liver transcriptome revealed a marked shift in Runx1 alternative splicing with a substantial decrease in exon 6 inclusion (Fig. 2). This impact on exon 6 splicing was highly selective in that splicing of all other Runx1 exons in the Pcbp2$^{-/-}$ fetal liver was unchanged and consistent with the unique presence of a C-rich PPT 5′ to the exon 6 splice site (27) (Fig. 4B). These findings prompted us to determine the *in vivo* physiological function of Runx1 exon 6 by generating a Runx1 locus that excluded exon 6 (Fig. 5). Mice homozygous for the Runx1ΔE6 mutation had a marked impairment in definitive erythroid lineage maturation in the embryonic liver (Fig. 6) that was remarkably

FIG 7 Legend (Continued)
by qPCR for primitive and definitive hemoglobin mRNA expression. Normalized expression of mRNAs from WT mice was defined as 1.0 in each case. The means and standard errors for each genotype are shown (minimum of three biological replicates per genotype). Statistical significance was determined by 2-sided Student's *t* test (*, $P < 0.05$; **, $P < 0.01$; ***, $P < 0.001$; ****, $P < 0.0001$). Hbb-bt, hemoglobin beta, adult t chain; Hba-a1, hemoglobin alpha, adult chain 1; Hbb-y, hemoglobin Y, beta-like embryonic chain; Hbb-bh1, hemoglobin Z, beta-like embryonic chain.

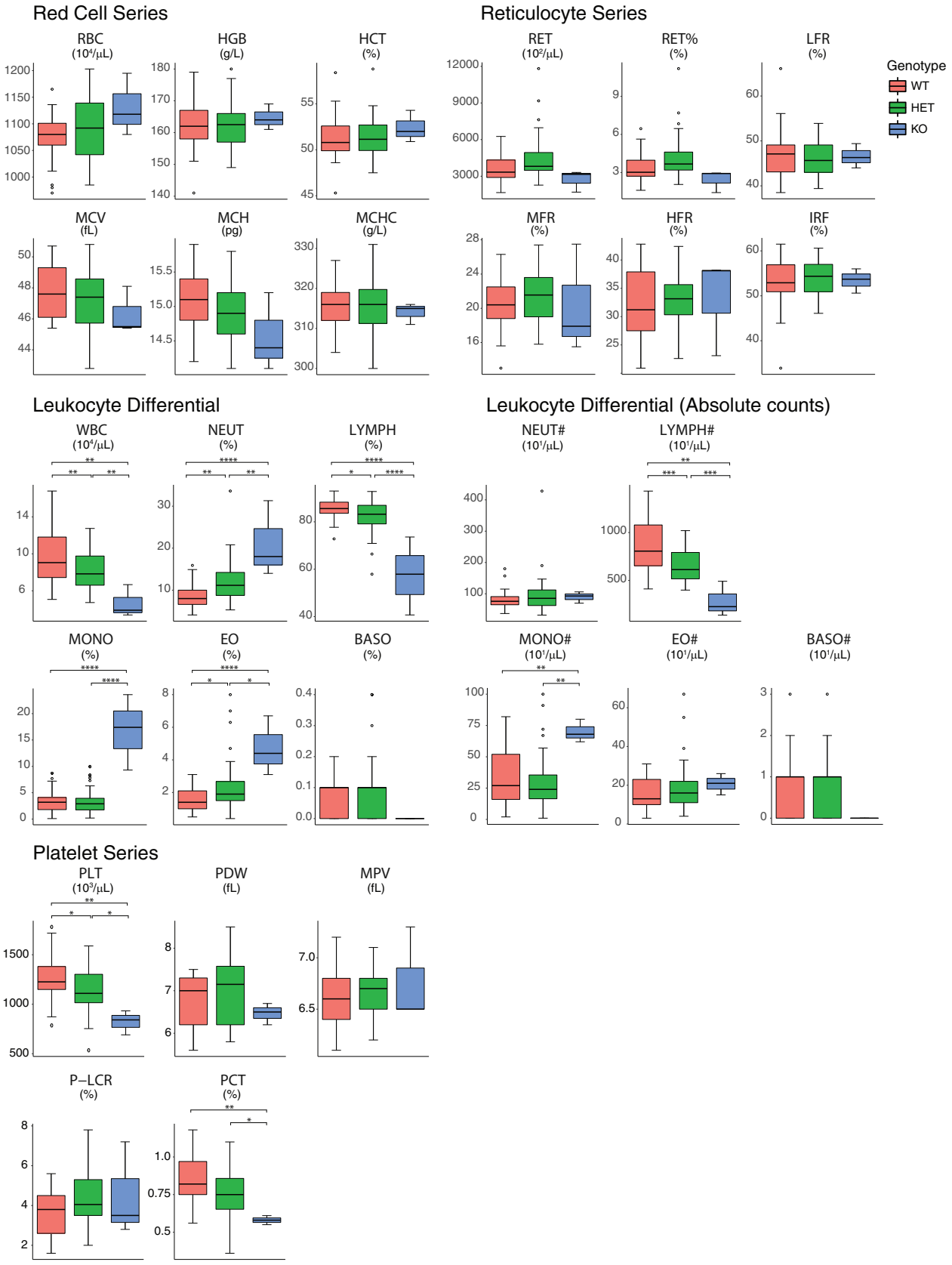

FIG 8 Runx1$^{\Delta E6/\Delta E6}$ adult mice have lymphopenia and thrombocytopenia with sparing of the erythroid series. Histograms show complete blood count data obtained by submandibular vein venipuncture from 8-week-old mice. Data are partitioned based on cell class and further subdivided by measured parameter. Red blood cell series abbreviations: RBC, red blood cell; Hgb, hemoglobin; Hct, hematocrit; MCV, mean corpuscular volume;

(Continued on next page)

similar to that seen in Pcbp2$^{-/-}$ mouse embryos (25). In contrast, Runx1$^{+/\Delta E6}$ mice had no discernible definitive erythroid phenotype in fetal liver or adult animals (Fig. 6 and 8), arguing against a dominant-negative effect of the Runx1ΔE6 mutant allele upon erythroid ontogeny. We observed a small increase in total Runx1 protein in Runx1$^{+/\Delta E6}$ and Runx1$^{\Delta E6/\Delta E6}$ fetal liver compared to levels for the wild type (Fig. 5E). Thus, it is possible that Runx1 overexpression is contributing to the observed erythroid phenotype. Importantly, however, we observed that the difference between Runx1 total protein expression in Runx1$^{+/\Delta E6}$ and Runx1$^{\Delta E6/\Delta E6}$ is modest (~0.2-fold), yet the impact of Runx1$^{\Delta E6/\Delta E6}$ homozygosity on fetal liver definitive erythropoiesis, where full-length Runx1 expression is fully lost, is markedly deleterious. This suggests that the definitive erythroid phenotype in Runx1$^{\Delta E6/\Delta E6}$ mice stems from loss of exon 6 rather than altered steady-state Runx1 total protein expression. The impairment of hematopoietic stem cell function in Runx1ΔE6 homozygote embryos was highlighted in a series of *ex vivo* burst-forming colony assays (BFU-E) and erythroid colony formation (CFU-E) assays (Fig. 7C). These data reveal strong correlations in the impacts of Pcbp2$^{-/-}$ and Runx1$^{\Delta E6/\Delta E6}$ genotypes on embryonic erythroid development.

Runx1 exon 6 deletion in mice has a milder phenotype than either the Pcbp2 or Runx1 null allele. Runx1 germ line inactivation results in a lethal phenotype at E12.5 characterized by embryonic hemorrhage, a complete loss of definitive hematopoiesis, and relative sparing of primitive hematopoiesis (10, 11). Similarly, Pcbp2 null embryos lose viability at E13.5, manifesting widespread hemorrhage associated with selective impacts on definitive erythroblast maturation and megakaryocyte development (25). In sharp contrast, Runx1$^{\Delta E6/\Delta E6}$ mice survive to parturition (Table 1). Runx1$^{\Delta E6/\Delta E6}$ embryos, like Runx1 and Pcbp2 null embryos, display a specific defect in development of the definitive erythroid lineage (Fig. 5) and decreased numbers and function of definitive myeloid progenitors (Fig. 7A to C). This indicates that Runx1 exon 6 selectively impacts definitive hematopoiesis in the embryonic liver while preserving other functions critical to embryonic viability.

The disparity between the marked impairment in fetal liver erythropoiesis and an essentially normal adult erythropoiesis in Runx1$^{\Delta E6/\Delta E6}$ mice points to a robust capacity in the mouse to overcome a substantial embryonic delay in erythron development (Fig. 8). This observation is in accord with reports demonstrating impaired early erythropoiesis in conjunction with normal adult red blood cell metrics in conditional Runx1 (Vav-cre) knockout mice (53, 54). Other studies exploring the impact of inducible Runx1 gene deletion upon adult hematopoiesis similarly demonstrated normal steady-state peripheral blood red blood cell populations (37, 55). Because the erythron has robust compensatory mechanisms for a variety of physiological stresses, notably the ability to dramatically increase erythropoietin synthesis to enhance erythroid differentiation and expansion (56, 57), we speculate that these *in vivo* mechanisms are intact and operative in surviving Runx1$^{\Delta E6/\Delta E6}$ mice. In summary, the Runx1ΔE6 mutant mouse model has demonstrated that Runx1 exon 6 is critical for normal progression of fetal liver definitive erythropoiesis but is dispensable for maintenance of steady-state erythropoiesis in adult mice.

Hematopoietic stem cells in Runx1$^{\Delta E6/\Delta E6}$ embryos have significant numerical and functional impairments. Similar to mice with germ line Runx1 deletion (Runx1$^{-/-}$) and mice with compartmentalized Runx1 genetic ablation in early hematopoietic progenitors (10, 54), the Runx1$^{\Delta E6/\Delta E6}$ E14.5 embryos displayed reduced Lin$^-$ Sca1$^+$ c-Kit$^+$ stem cell populations and markedly decreased MPP, CMP, and GMP progenitor lineages (Fig. 7A and B). This corresponded with a nearly complete absence of myeloid and

FIG 8 Legend (Continued)
MCH, mean corpuscular hemoglobin; MCHC, mean corpuscular hemoglobin content. Reticulocyte series abbreviations: RET, reticulocyte absolute count; RET%, reticulocyte percentage; LFR, low fluorescence ratio; MFR, middle fluorescence ratio; HFR, high fluorescence ratio; IRF, immature reticulocyte fraction. Leukocyte differential abbreviations: WBC, white blood cells; NEUT, neutrophils; LYMPH, lymphocytes; MONO, monocytes; EO, eosinophils; BASO, basophils; NEUT#, absolute neutrophil count; LYMPH#, absolute lymphocyte count; MONO#, absolute monocyte count; EO#, absolute eosinophil count; BASO#, absolute basophil count. Platelet series abbreviations: PLT, absolute platelet count; PDW, platelet distribution width; MPV, mean platelet volume; P-LCR, platelet larger cell ratio; PCT, plateletcrit.

erythroid colony formation ability (Fig. 7C). These data demonstrate that Runx1 exon 6 encodes activities critical for both maintenance and function of multipotent and myeloid progenitor cells in the embryo. In conjunction with the observation that Runx1$^{\Delta E6/\Delta E6}$ adult mice have defects in nonerythroid hematopoietic lineages (Fig. 8), these data further define a specific mechanistic role of the exon 6-encoded segment on embryonic and adult definitive hematopoiesis.

Although there was a stepwise reduction in MPP and CMP populations in Runx1ΔE6 heterozygous mice, we did not observe a functional difference in the ability of fetal liver stem cells from these mice to generate *ex vivo* early myeloid or erythroid colonies. This result may be attributable to a well-described Runx1 gene dosage effect in hematopoiesis (51). For example, a Runx1 haploinsufficiency phenotype in mice impacts the timing and spatial distribution of hematopoietic stem cells (58) and decreases erythroid and myeloid progenitor levels in mutant embryos (10, 59). Based on these data, we speculate that mechanisms that control the splicing activity of exon 6 in Runx1 isoforms operate to maintain a critical balance between populations of pluripotent HSCs and more committed progenitors in the mouse fetal liver.

The polypyrimidine tract (PPT) at the Runx1 exon 6 splice acceptor is markedly enriched for cytosine content (Fig. 4B). We have previously demonstrated that PPTs with such C-rich structures enhance cassette exon retention in a Pcbp-dependent manner (27). Our prior studies further demonstrated that this preference for C-rich structures contrasts with the U-rich binding activity of U2AF65. U2AF65 is the canonical splice acceptor PPT binding protein splice factor that is active at the great majority of mammalian splice sites. The mechanism by which Pcbps enhance splicing of C-rich splice acceptors is the direct interaction and recruitment of splicing factors associated with the U2 snRNP complex (27). In this way, Pcbps operate to replace U2AF65 as the PPT binding protein at C-rich splice acceptors and facilitate spliceosome assembly. Our analysis of a subset of PPT binding proteins revealed that Pcbp2 function served to specifically enhance exon 6 inclusion in Runx1 splicing (Fig. 4C). This control is likely mediated by direct *in vivo* binding of Pcbp2 to the Runx1 exon 6 PPT. This model is supported by eCLIP data (ENCODE project experiment ENCSR339FUY [60]) demonstrating the direct binding of Pcbp2 to this site in a hepatocellular carcinoma cell line. Short interfering RNA (siRNA) knockdown of Pcbp1 had a modest effect on Pcbp2 protein expression and resulted in a small increase in exon 6 skipping (Fig. 4D). Therefore, the modest impact of Pcbp1 knockdown on Runx1 exon 6 skipping may be attributable to a crossover impact of the Pcbp1 siRNA on Pcbp2 levels. The apparent negative effect of hnRNPK on exon 6 splicing that we observed (Fig. 4D) is in keeping with reports describing this closely related KH domain poly(C) binding protein as a repressor of Runx1 exon 6 splicing during neuronal differentiation and could reflect direct competition of hnRNPK with Pcbp2 for PPT binding (61). We conclude from these studies that the mechanistic role of Pcbp2 during murine fetal liver development and in erythroid lineage cells across mammalian species is conserved and serves to specifically enhance functional splicing of Runx1 exon 6.

Runx1 is a DNA binding protein that can function as a transcriptional repressor through direct association/recruitment of corepressors such as the Sin3a deacetylase complex (62–66). Runx1 binding to the Sin3a complex occurs by interactions with the protein domain encoded by Runx1 exon 6; Runx1 proteins lacking the exon 6-encoded domain fail to repress transcription in cell-based assays (65). Recent studies have demonstrated that both Runx1 and the Sin3a deacetylase complex are components of the Bcl11a corepressor complex that maintains fetal hemoglobin silencing in adult erythroid cells (62). In addition, human Sin3a allelic variants associated with lower Sin3a expression and higher fetal hemoglobin levels in adult erythroid cells have been described (67). We observe that both the Runx1$^{\Delta E6/\Delta E6}$ and Pcbp2$^{-/-}$ embryos had increased embryonic hemoglobin gene expression in fetal liver, with proportional reductions in definitive hemoglobin gene expression (Fig. 1B and 6C). Whether these changes relate directly to alterations in Bcl11A function remains to be explored.

Runx1 has a well-documented role in the expansion and maintenance of lymphoid

and platelet populations (37, 54, 55, 68, 69). Adult Runx1$^{\Delta E6/\Delta E6}$ mice demonstrate a similar phenotype of cytopenias in blood lymphocyte and platelet populations (Fig. 8). The lymphoid transcription factor Ets-1 heterodimerizes with Runx1 to assemble a transcriptional activator complex (70). The Runx1 exon 6-encoded protein segment encompasses one of two Ets-1-interacting domains required for full transcriptional activity of the Runx1-Ets-1 heterodimer. While Runx1 isoforms lacking exon 6 can still bind Ets-1, the heterodimer has significantly reduced transactivation ability compared to that of the exon 6-containing isoform (70). These data lead us to suggest that the decreased lymphocyte numbers observed in the Runx1ΔE6 mice reflect the assembly of functionally defective Runx1-Ets-1 heterodimers at critical promoter sites.

Arginine methylation by PRMT1 and PRMT4 occurs at three sites in exon 6 (31, 71). Opposing methylation-dependent effects on Runx1 transcriptional activity appear to occur at different stages of myeloid development. Methylation of Runx1 by PRMT4 in HSCs triggers formation of a multiprotein repressor complex that suppresses expression of the microRNA Mir-223, an activity essential for normal myeloid differentiation of human CD34$^+$ cord blood cells (71). In contrast, Runx1 methylation also releases Runx1 from Sin3A transcriptional repressor complexes and increases Runx1 transcriptional activity of at least two hematopoietic target gene promoters, CD41 and PU.1 (31), in CD34$^+$ cells stimulated to differentiate toward the myeloid lineage. Given the complex and stage-specific dependence of Runx1 methylation and its consequences on Runx1 activity during myelopoiesis, it is conceivable that the Runx1ΔE6 phenotypes described here arise in whole, or in part, due to abnormal posttranslational methylation of the Runx1 protein.

Although Runx1 exon 6 is not essential for fetal survival, Runx1$^{\Delta E6/\Delta E6}$ mice had significantly reduced neonatal fitness (Table 1). Diminished postpartum survival has been reported for other mouse lines carrying conditional Runx1 gene deletion in hematopoietic lineages (53, 54). Our data revealed that Runx1$^{\Delta E6/\Delta E6}$ neonates had normal birth weight compared to littermates and were capable of nursing based upon the presence of normal milk spots, arguing against intrauterine growth retardation or major defects in oral motor function (data not shown). Because Runx1 is a critical factor in neuronal differentiation, proliferation, and migration during development (72–76), we speculate that neurological deficits or impairments in the enteric nervous system, unassociated with the defined hematopoietic abnormalities (53), in some manner diminish neonatal fitness.

In summary, these data highlight the importance of Pcbp2 to the progression of embryonic hematopoiesis and the activation of the definitive erythroid lineage. The impact of Pcbp2 on splicing of Runx1 exon 6 and the hematologic phenotype of embryos exclusively expressing the Runx1ΔE6 protein support a mechanistic linkage between the defect in definitive erythroid development in Pcbp2$^{-/-}$ embryos and the impact of Pcbp2 on Runx1 structure and function. What is now of clear interest is to address how these splicing controls may themselves be modulated during development and/or in response to environmental stimuli. Pcbp RNA binding activities can be controlled by intracellular compartmentalization, phosphorylation in response to transforming growth factor beta (TGFβ) signaling, interactions with other cytosolic factors, and signals emanating from nutritional status (77–79). While it is clear that Pcbp proteins are critical regulators of alternative splicing in the erythroid lineage, as demonstrated by this study and earlier reports (27), subsequent studies designed to extend our understanding of the mechanisms controlling Pcbp RNA functions during erythropoiesis will further contribute to models of the pathways that control these developmental processes.

MATERIALS AND METHODS

MAJIQ. TruSeq stranded mRNA sequencing libraries were generated from Pcbp2$^{-/-}$ 12.5-day-postcoitus (dpc) fetal liver and wild-type littermates and sequenced as previously reported (data sets are available at the Gene Expression Omnibus [GEO] database under accession number GSE72491 [25]). Libraries from three wild-type and four Pcbp2$^{-/-}$ biological replicates were indexed, pooled, and sequenced in a single lane. RNA-seq reads were aligned using STAR (80). Differential alternative splicing analysis was performed using MAJIQ (v 1.0.4) (28). Local splicing variations (LSVs) were defined, and

high-confidence splicing changes were determined by selecting those with one or more junctions with P($\Delta\Psi > 0.2$) of >0.95, where $\Delta\Psi$ is the relative change in the percent selected index (PSI, Ψ) for each junction involved in an LSV. LSVs detected in only one of the replicates per genotype were excluded.

Gene set data analysis. Log_2 fold changes from RNA-seq of Pcbp2$^{-/-}$ versus wild-type fetal liver (25) were intersected with lists of primitive and definitive erythroid genes defined by Greenfest-Allen et al. (5). Only genes with an essentiality score of $\geq$1.8 were used for analysis. Similarly, $\log_2$ fold changes from Pcbp2$^{-/-}$ versus wild-type fetal liver RNA-Seq (25) were intersected with lists of (i) genes that are binding targets of Runx1 as defined by ChIP-seq and their correlation with Runx1 expression during embryonic stem cell differentiation and (ii) differentially expressed genes in VE-cadherin^{+} cells from Runx1$^{-/-}$ embryos reported by Tanaka et al. (32). Results were visualized as cumulative distribution functions of the $\log_2$ fold changes for each subset or as box plots, and statistics were performed with the Mann-Whitney U test.

Cell culture and siRNA transfection. K562 cells were cultured in RPMI 1640 medium supplemented with 10% fetal bovine serum (HyClone) and antibiotic/antimycotic (Gibco) at 37°C in a standard humidified 5% CO_2 incubator. K562 cells were transfected with siRNAs using Nucleofector V (Amaxa) as previously described (81). siRNAs targeting U2AF65, PCBP1, PCBP2, and a negative control (medium GC content) were as previously described (27). The sequences of the siRNAs to PCBP1, PCBP2, and U2AF65 were as previously described (27). siRNAs to PTBP1 (HSS143520, HSS143518, and HSS183787) and to hnRNPK (HSS179311, HSS179312, and HSS179313) were purchased from Invitrogen. In each case three distinct siRNAs targeting the indicated mRNA were pooled prior to transfection. Cells were cultured for 3 days after transfection prior to harvesting for analysis.

Mouse studies. All mouse studies were conducted in accordance with protocols approved by the Institutional Animal Care and Use Committee at the Perelman School of Medicine at the University of Pennsylvania and at the Children's Hospital of Philadelphia. All mice were housed in standard cages within a barrier facility under 12 h of on/off light cycling conditions and were given *ad libitum* access to standard mouse chow and water. Euthanasia was achieved by an approved protocol of carbon dioxide inhalation followed by cervical dislocation. The Pcpb2 knockout mouse line used in this study was previously described (25).

Targeted deletion of mouse Runx1 exon 6 using Cas9 endonucleases. Standard CRISPR-Cas9-mediated gene editing (82) was utilized to generate an exon 6-deleted mutant allele of the Runx1 locus (Runx1ΔE6). Single-guide RNAs (sgRNAs) targeting the introns flanking exon 6 were selected based on principles that minimize off-target effects as described in Doench et al. (83). The intron 5 sgRNA (Runx1E6_gRNA.254, GGGCACCGAGTCCCAGACTG) was designed to target chromosome 16 (Chr 16) coordinates 92644590 to 92644609 (*Mus musculus* genomic assembly mm10) and the intron 6 sgRNA (Runx1E6_gRNA.121, GAAACCCCGCAGCATCAGCT) targeted to Chr 16, positions 92644031 to 92644050 (Fig. 5A). Synthesized sgRNAs and tracrRNA (Alt-R CRISPR-Cas9 tracrRNA; number 1072532) were obtained from Integrated DNA Technologies (CA). sgRNA and tracrRNA were diluted to 50 μM (final concentration in duplex mix) in nuclease-free duplex buffer (number 11-01-03-01; IDT), and the annealed sgRNA-tracrRNA duplexes were generated by heating for 10 min at 95°C and cooling to room temperature. Each sgRNA-tracr duplex was diluted to 75 ng/μl. The capped and polyadenylated Cas9 mRNA (number L-7206; TriLink BioTechnologies) was diluted to 100 ng/μl final concentration in microinjection buffer (10 mM Tris-HCl, pH 7.4, 0.1 mM EDTA) and stored at −80°C until microinjection. Cytoplasmic microinjection was performed in single-cell embryos derived from mating male and female B6SJLF1/J mice (stock number 100012; Jackson Laboratory) at the Transgenic and Chimeric Mouse Facility of the University of Pennsylvania. Embryos were transferred into pseudopregnant CD-1 females (Charles River Production), and resultant pups were screened for mutations by PCR (forward primer, Runx1E6_delta_995_for, TAGTGTCTGCCCACCCGAG; reverse primer, Runx1E6_delta_995_rev, AGATTAAA CCGAAGGTGGGTTG) (Fig. 5B). PCR products were subcloned for sequencing using a TOPO TA cloning kit (number K4500J10; Invitrogen). A minimum of 10 clones were Sanger sequenced for each pup to confirm exon 6 deletion (Fig. 5B). The founder line was designated Runx1ΔE6.

Western blotting. (i) Fetal liver. Fetal livers from three E14.5 embryos per genotype were obtained from CO_2-euthanized dams. Gestational dating was verified by crown-rump measurements done *ex vivo* at the time of embryo harvest. Embryos were kept in ice-cold 1× phosphate-buffered saline (PBS) during dissection for anesthesia. The liver tissue was homogenized by mortar and pestle in ice-cold lysis buffer (1× PBS, pH 7.2, 0.1% SDS, 0.5% IGEPAL CA-630, protease inhibitor cocktail [11836170001; Roche]) with prechilled instruments and tubes. SDS-PAGE and Western blotting were performed as described previously (25). Fetal liver proteins were visualized with fluorophore-conjugated secondary antibodies at 1:15,000 in 1× PBS, pH 7.2, 0.1% Tween, 0.1% SDS (IRDye 800CW anti-rabbit antibody; number 925-32213), and IRDye 680RD anti-mouse antibody (925-68072; LI-COR, Lincoln, NE). Signal density was measured on a LI-COR Odyssey CLx imaging platform. Relative expression of full-length and truncated Runx1 signals was determined by normalization to signal density of the housekeeping glyceraldehyde-3-phosphate dehydrogenase (GAPDH) gene using Image Studio, version 3.1.

(ii) Transfected cells. For K562 transfection experiments, total cellular protein extracts were prepared from TRIzol-dissolved transfected K562 cells according to the manufacturer's instructions (TRIzol reagent; 15596; Invitrogen). Extracts were separated by SDS-PAGE on a 4 to 12% NuPAGE gel (Invitrogen) and electroblotted to nitrocellulose membranes (Protran BA 85; Schleicher & Schuell) for 1 h at 150 mA in transfer buffer (20 mM Tris, 150 mM glycine, 20% methanol) using a Semi-phor transfer apparatus (Hoefer). The membranes were blocked in 1% nonfat milk in 1× PBS for 1 h at room temperature, followed by 3 h with primary antisera (see Table S1 in the supplemental material). Goat anti-rabbit immunoglobulin G–horseradish peroxidase (IgG-HRP) secondary antibody (7074S; Cell Signaling) and

sheep anti-mouse IgG–HRP secondary antibody (NA931V; GE Healthcare) were used at a 1:5,000 dilution. Proteins were visualized by enhanced chemiluminescence (RPN2109; GE Healthcare).

RNA analyses. Normalized mRNA expression from Pcbp2 wild-type and Pcbp2 knockout E12.5 fetal liver was computed from RNA-seq data reported by Ghanem et al. (GSE72491) (25). In this report, DESeq2 was used to identify differentially expressed genes ($P < 0.001$) (84).

RT-PCR analyses. Total RNA from K562 cells or mouse fetal liver was purified by TRIzol reagent (15596026; Invitrogen) and then treated with DNase I (Invitrogen) and reverse transcribed using oligo(dT)$_{12–18}$ priming (18418012; Invitrogen), Moloney murine leukemia virus reverse transcriptase (Promega), and 1× Moloney murine leukemia virus reverse transcription (RT) buffer (Promega) according to the manufacturer's instructions. The reaction mixture was incubated at 37°C for 1 h, and cDNA was used as a template for PCR. The forward primer (20 pmol) was end labeled by incubation with [γ^{32}-P]ATP and T4 PNK kinase (New England BioLabs). The PCR included 1 μl of the reverse transcription product, 0.2 mM deoxynucleoside triphosphates (dNTPs), 1.5 mM $MgCl_2$, 1 pmol of the labeled forward primer, 20 pmol of each unlabeled forward and reverse primer, 0.25 U of AmpliTaq (PerkinElmer), and 1× PCR buffer II (PerkinElmer) in a 25-μl reaction volume. The number of PCR cycles in each study was adjusted to be in the linear range. Samples were electrophoresed on a denaturing 6% polyacrylamide gel and quantified by PhosphorImager (ImageQuant; Molecular Dynamics). Runx1 exon 6 alternative splicing efficiency was determined by calculating the inclusion level (percent) of this exon in all isoforms. Human Runx1 and mouse Runx1 RT-PCR primers for exon 6 alternative splicing analysis are detailed in Table S2.

qPCR. Fetal liver RNA from E12.5 and E14.5 embryos was purified per the manufacturer's protocol using TRIzol (15596026; Invitrogen). Four hundred nanograms of total RNA was DNase I treated and used for cDNA synthesis. RNA was primed with oligo(dT)$_{12–18}$ and random hexamers and reverse transcribed for 50 min at 50°C with Superscript III per the vendor's protocol (18080085; Invitrogen). cDNA was diluted 10-fold, and 2 μl of diluted cDNA was used for each 20-μl quantitative PCR (qPCR; Fast SYBR green mix; 4385612; Applied Biosystems). Amplification was performed on an Applied Biosystems 7900HT Fast real-time PCR. Normalized relative quantification was performed as previously described (25). qPCR target genes and primer sequences are detailed in Table S2.

Complete blood counts. Blood for steady-state peripheral blood counts were obtained from 8-week-old adult mice by submandibular vein phlebotomy. Blood was mixed by gentle inversion 10 times in potassium-EDTA tubes (363706; Becton Dickinson) to anticoagulate. Complete blood count, leukocyte differential, and reticulocyte counts were obtained on a Sysmex XT-2000iV automated hematology analyzer in the Translational Core Laboratory at the Children's Hospital of Philadelphia Research Institute.

Flow cytometry. Murine hematopoietic cells were isolated from E14.5 fetal livers. Viability of all embryos at the time of harvest was confirmed by visualization of a heartbeat. Livers were dissected and immediately placed into ice-cold PBS supplemented with 2% fetal bovine serum, 2.5 mM EDTA, and 1% penicillin-streptomycin (PenStrep). Single-cell suspensions were generated by passage through 40-μm prechilled cell strainers. Cells were washed with PBS and resuspended in 1:500 Live/Dead aqua in PBS and incubated at 4°C for 30 min. Cells were then resuspended in PBS with fluorophore-conjugated antibodies (Table S1) and incubated in the primary antibody stain on ice for 1 h in the dark, washed with PBS, and then resuspended in supplemented PBS for fluorescence-activated cell sorter (FACS) analysis. For erythroid differentiation analysis by CD71 and Ter119 staining, a minimum of 100,000 cells per sample were captured on an LSR Fortessa flow cytometer (BD Biosciences) in the Flow Cytometry Core Laboratory of The Children's Hospital of the Philadelphia Research Institute, and data were analyzed using FlowJo. The S staging system for erythroid maturation (stages S0 through S5) was used to define gates for quantitation of erythroid progenitors as described previously (36). For stem cell and myeloid progenitor analysis, fetal liver cells prepared as described above were stained with a cell viability dye per the manufacturer's instructions (Live/Dead fixable aqua; L34957; Invitrogen), washed, and then incubated with a primary antibody stain mix (c-Kit, ScaI, CD34, Flt3, FcgrIII, and mature lineage markers [CD3, B220, Gr-1, and Ter119]; Table S1) and washed before FACS analysis (38).

CFU assays. The ability of fetal liver stem cells to differentiate and produce myeloid progenitor cells was quantified as CFU (39). E14.5 mouse fetal livers were harvested into 1 ml PBS–2% FBS–PenStrep–2.5 mM EDTA and processed into single-cell suspensions by triturating and straining through 40-μm filters. Nucleated cells were counted by hemocytometer using methylene blue and 3% acetic acid stain (07060; Stemcell Technologies). Fetal liver cells were cultured in triplicate for each genotype in methylcellulose medium containing growth factors (03434; Stemcell Technologies) at 10,000 cells per 1 ml medium in a 35-mm dish to measure BFU-E, CFU-GM, and CFU-GEMM colonies. Cells were cultured for 7 days at 37°C and 5% CO_2 in a humidified incubator. Colonies were visualized by bright-field microscopy and scored in a blinded manner based on parameters set forth in the manufacturer's instructions (mouse CFU assays using Methocult, technical manual version 3.5.0; Stemcell Technologies). CFU-E colonies were cultured in methylcellulose supplemented with erythropoietin (03334; Stemcell Technologies) and scored on day 2.

SUPPLEMENTAL MATERIAL

Supplemental material for this article may be found at https://doi.org/10.1128/MCB.00175-18.

SUPPLEMENTAL FILE 1, PDF file, 0.1 MB.

SUPPLEMENTAL FILE 2, XLSX file, 0.1 MB.

ACKNOWLEDGMENTS

We are grateful for productive discussions with Nancy Speck, Johanna Tober, Wei Tong, Mortimer Poncz, and members of their respective laboratories.

This work was supported by NIH R01 HL065449 (S.A.L.) and NIH K08-DK102957 (L.R.G.).

Authors made the following contributions: conceptualization, L.R.G. and S.A.L.; methodology, L.R.G. and S.A.L.; formal analysis, L.R.G., I.M.S., M.G., Y.B., and S.A.L.; investigation, L.R.G., A.K., I.M.S., X.J., M.G., N.N., G.A., and M.M.; writing (original draft), L.R.G., I.M.S., X.J., M.G., and S.A.L.; writing (review and editing), L.R.G. and S.A.L.; supervision, L.R.G. and S.A.L.; funding acquisition, L.R.G. and S.A.L.

We have no conflicts of interest to declare.

REFERENCES

1. Palis J. 2014. Primitive and definitive erythropoiesis in mammals. Front Physiol 5:3. https://doi.org/10.3389/fphys.2014.00003.
2. Ji RP, Phoon CKL, Aristizábal O, McGrath KE, Palis J, Turnbull DH. 2003. Onset of cardiac function during early mouse embryogenesis coincides with entry of primitive erythroblasts into the embryo proper. Circ Res 92:133–135. https://doi.org/10.1161/01.RES.0000056532.18710.C0.
3. Kingsley PD, Malik J, Fantauzzo KA, Palis J. 2004. Yolk sac-derived primitive erythroblasts enucleate during mammalian embryogenesis. Blood 104:19–25. https://doi.org/10.1182/blood-2003-12-4162.
4. Swiers G, Rode C, Azzoni E, de Bruijn MFTR. 2013. A short history of hemogenic endothelium. Blood Cells Mol Dis 51:206–212. https://doi.org/10.1016/j.bcmd.2013.09.005.
5. Greenfest-Allen E, Malik J, Palis J, Stoeckert CJ. 2013. Stat and interferon genes identified by network analysis differentially regulate primitive and definitive erythropoiesis. BMC Syst Biol 7:38. https://doi.org/10.1186/1752-0509-7-38.
6. Kingsley PD, Greenfest-Allen E, Frame JM, Bushnell TP, Malik J, McGrath KE, Stoeckert CJ, Palis J. 2013. Ontogeny of erythroid gene expression. Blood 121:e5–e13. https://doi.org/10.1182/blood-2012-04-422394.
7. Palis J, Malik J, McGrath KE, Kingsley PD. 2010. Primitive erythropoiesis in the mammalian embryo. Int J Dev Biol 54:1011–1018. https://doi.org/10.1387/ijdb.093056jp.
8. Borg J, Patrinos GP, Felice AE, Philipsen S. 2011. Erythroid phenotypes associated with KLF1 mutations. Haematologicaae 96:635–638. https://doi.org/10.3324/haematol.2011.043265.
9. Vegiopoulos A, García P, Emambokus N, Frampton J. 2006. Coordination of erythropoiesis by the transcription factor c-Myb. Blood 107:4703–4710. https://doi.org/10.1182/blood-2005-07-2968.
10. Wang Q, Stacy T, Binder M, Marin-Padilla M, Sharpe AH, Speck NA. 1996. Disruption of the Cbfa2 gene causes necrosis and hemorrhaging in the central nervous system and blocks definitive hematopoiesis. Proc Natl Acad Sci U S A 93:3444–3449. https://doi.org/10.1073/pnas.93.8.3444.
11. Okuda T, van Deursen J, Hiebert SW, Grosveld G, Downing JR. 1996. AML1, the target of multiple chromosomal translocations in human leukemia, is essential for normal fetal liver hematopoiesis. Cell 84:321–330. https://doi.org/10.1016/S0092-8674(00)80986-1.
12. Ostareck-Lederer A, Ostareck DH. 2004. Control of mRNA translation and stability in haematopoietic cells: the function of hnRNPs K and E1/E2. Biol Cell 96:407–411. https://doi.org/10.1016/j.biolcel.2004.03.010.
13. Ostareck DH, Ostareck-Lederer A, Wilm M, Thiele BJ, Mann M, Hentze MW. 1997. mRNA silencing in erythroid differentiation: hnRNP K and hnRNP E1 regulate 15-lipoxygenase translation from the 3′ end. Cell 89:597–606. https://doi.org/10.1016/S0092-8674(00)80241-X.
14. Williamson AJK, Smith DL, Blinco D, Unwin RD, Pearson S, Wilson C, Miller C, Lancashire L, Lacaud G, Kouskoff V, Whetton AD. 2008. Quantitative proteomics analysis demonstrates post-transcriptional regulation of embryonic stem cell differentiation to hematopoiesis. Mol Cell Proteomics 7:459–472. https://doi.org/10.1074/mcp.M700370-MCP200.
15. Lodish HF, Small B. 1976. Different lifetimes of reticulocyte messenger RNA. Cell 7:59–65. https://doi.org/10.1016/0092-8674(76)90255-5.
16. Weiss IM, Liebhaber SA. 1994. Erythroid cell-specific determinants of alpha-globin mRNA stability. Mol Cell Biol 14:8123–8132. https://doi.org/10.1128/MCB.14.12.8123.
17. Makeyev AV, Chkheidze AN, Liebhaber SA. 1999. A set of highly conserved RNA-binding proteins, alphaCP-1 and alphaCP-2, implicated in mRNA stabilization, are coexpressed from an intronless gene and its intron-containing paralog. J Biol Chem 274:24849–24857. https://doi.org/10.1074/jbc.274.35.24849.
18. Makeyev AV, Liebhaber SA. 2002. The poly(C)-binding proteins: a multiplicity of functions and a search for mechanisms. RNA 8:265–278. https://doi.org/10.1017/S1355838202024627.
19. Chaudhury A, Chander P, Howe PH. 2010. Heterogeneous nuclear ribonucleoproteins (hnRNPs) in cellular processes: Focus on hnRNP E1's multifunctional regulatory roles. RNA 16:1449–1462. https://doi.org/10.1261/rna.2254110.
20. Philpott CC. 2012. Coming into view: eukaryotic iron chaperones and intracellular iron delivery. J Biol Chem 287:13518–13523. https://doi.org/10.1074/jbc.R111.326876.
21. Kiledjian M, Wang X, Liebhaber SA. 1995. Identification of two KH domain proteins in the alpha-globin mRNP stability complex. EMBO J 14:4357–4364.
22. Waggoner SA, Liebhaber SA. 2003. Identification of mRNAs associated with alphaCP2-containing RNP complexes. Mol Cell Biol 23:7055–7067. https://doi.org/10.1128/MCB.23.19.7055-7067.2003.
23. Ji X, Kong J, Liebhaber SA. 2011. An RNA-protein complex links enhanced nuclear 3′ processing with cytoplasmic mRNA stabilization. EMBO J 30:2622–2633. https://doi.org/10.1038/emboj.2011.171.
24. Ji X, Kong J, Carstens RP, Liebhaber SA. 2007. The 3′ untranslated region complex involved in stabilization of human alpha-globin mRNA assembles in the nucleus and serves an independent role as a splice enhancer. Mol Cell Biol 27:3290–3302. https://doi.org/10.1128/MCB.02289-05.
25. Ghanem LR, Kromer A, Silverman IM, Chatterji P, Traxler E, Penzo-Mendez A, Weiss MJ, Stanger BZ, Liebhaber SA. 2015. The poly(C) binding protein Pcbp2, and its retrotransposed derivative Pcbp1, are independently essential to mouse development. Mol Cell Biol 36:304–319. https://doi.org/10.1128/MCB.00936-15.
26. Woolthuis CM, Park CY. 2016. Hematopoietic stem/progenitor cell commitment to the megakaryocyte lineage. Blood 127:1242–1248. https://doi.org/10.1182/blood-2015-07-607945.
27. Ji X, Park JW, Bahrami-Samani E, Lin L, Duncan-Lewis C, Pherribo G, Xing Y, Liebhaber SA. 2016. αCP binding to a cytosine-rich subset of polypyrimidine tracts drives a novel pathway of cassette exon splicing in the mammalian transcriptome. Nucleic Acids Res 44:2283–2297. https://doi.org/10.1093/nar/gkw088.
28. Vaquero-Garcia J, Barrera A, Gazzara MR, González-Vallinas J, Lahens NF, Hogenesch JB, Lynch KW, Barash Y. 2016. A new view of transcriptome complexity and regulation through the lens of local splicing variations. Elife 5:e11752. https://doi.org/10.7554/eLife.11752.
29. Huang H, Woo AJ, Waldon Z, Schindler Y, Moran TB, Zhu HH, Feng G-S, Steen H, Cantor AB. 2012. A Src family kinase-Shp2 axis controls RUNX1 activity in megakaryocyte and T-lymphocyte differentiation. Genes Dev 26:1587–1601. https://doi.org/10.1101/gad.192054.112.
30. Komeno Y, Yan M, Matsuura S, Lam K, Lo M-C, Huang Y-J, Tenen DG, Downing JR, Zhang D-E. 2014. Runx1 exon 6-related alternative splicing isoforms differentially regulate hematopoiesis in mice. Blood 123:3760–3769. https://doi.org/10.1182/blood-2013-08-521252.
31. Zhao X, Jankovic V, Gural A, Huang G, Pardanani A, Menendez S, Zhang J, Dunne R, Xiao A, Erdjument-Bromage H, Allis CD, Tempst P, Nimer SD. 2008. Methylation of RUNX1 by PRMT1 abrogates SIN3A binding and

potentiates its transcriptional activity. Genes Dev 22:640–653. https://doi.org/10.1101/gad.1632608.
32. Tanaka Y, Joshi A, Wilson NK, Kinston S, Nishikawa S, Göttgens B. 2012. The transcriptional programme controlled by Runx1 during early embryonic blood development. Dev Biol 366:404–419. https://doi.org/10.1016/j.ydbio.2012.03.024.
33. Thisted T, Lyakhov DL, Liebhaber SA. 2001. Optimized RNA targets of two closely related triple KH domain proteins, heterogeneous nuclear ribonucleoprotein K and alphaCP-2KL, suggest distinct modes of RNA recognition. J Biol Chem 276:17484–17496. https://doi.org/10.1074/jbc.M010594200.
34. Wahl MC, Will CL, Luhrmann R. 2009. The spliceosome: design principles of a dynamic RNP machine. Cell 136:701–718. https://doi.org/10.1016/j.cell.2009.02.009.
35. Yzaguirre AD, de Bruijn MFTR, Speck NA. 2017. The role of Runx1 in embryonic blood cell formation. Adv Exp Med Biol 962:47–64. https://doi.org/10.1007/978-981-10-3233-2_4.
36. Koulnis M, Pop R, Porpiglia E, Shearstone JR, Hidalgo D, Socolovsky M. 2011. Identification and analysis of mouse erythroid progenitors using the CD71/TER119 flow-cytometric assay. J Vis Exp 2011:2809.
37. Ichikawa M, Asai T, Saito T, Seo S, Yamazaki I, Yamagata T, Mitani K, Chiba S, Ogawa S, Kurokawa M, Hirai H. 2004. AML-1 is required for megakaryocytic maturation and lymphocytic differentiation, but not for maintenance of hematopoietic stem cells in adult hematopoiesis. Nat Med 10:299–304. https://doi.org/10.1038/nm997.
38. Challen GA, Boles N, Lin KK-Y, Goodell MA. 2009. Mouse hematopoietic stem cell identification and analysis. Cytometry A 75:14–24. https://doi.org/10.1002/cyto.a.20674.
39. Miller CL, Lai B. 2005. Human and mouse hematopoietic colony-forming cell assays. Methods Mol Biol 290:71–89.
40. Blouin MJ, De Paepe ME, Trudel M. 1999. Altered hematopoiesis in murine sickle cell disease. Blood 94:1451–1459.
41. Beauchemin H, Blouin M-J, Trudel M. 2004. Differential regulatory and compensatory responses in hematopoiesis/erythropoiesis in alpha- and beta-globin hemizygous mice. J Biol Chem 279:19471–19480. https://doi.org/10.1074/jbc.M309989200.
42. de Bruijn M, Dzierzak E. 2017. Runx transcription factors in the development and function of the definitive hematopoietic system. Blood 129:2061–2069. https://doi.org/10.1182/blood-2016-12-689109.
43. Draper JE, Sroczynska P, Tsoulaki O, Leong HS, Fadlullah MZH, Miller C, Kouskoff V, Lacaud G. 2016. RUNX1B expression is highly heterogeneous and distinguishes megakaryocytic and erythroid lineage fate in adult mouse hematopoiesis. PLoS Genet 12:e1005814. https://doi.org/10.1371/journal.pgen.1005814.
44. Levanon D, Groner Y. 2004. Structure and regulated expression of mammalian RUNX genes. Oncogene 23:4211–4219. https://doi.org/10.1038/sj.onc.1207670.
45. Bee T, Liddiard K, Swiers G, Bickley SRB, Vink CS, Jarratt A, Hughes JR, Medvinsky A, de Bruijn MFTR. 2009. Alternative Runx1 promoter usage in mouse developmental hematopoiesis. Blood Cells Mol Dis 43:35–42. https://doi.org/10.1016/j.bcmd.2009.03.011.
46. Miyoshi H, Ohira M, Shimizu K, Mitani K, Hirai H, Imai T, Yokoyama K, Soeda E, Ohki M. 1995. Alternative splicing and genomic structure of the AML1 gene involved in acute myeloid leukemia. Nucleic Acids Res 23:2762–2769. https://doi.org/10.1093/nar/23.14.2762.
47. Telfer JC, Rothenberg EV. 2001. Expression and function of a stem cell promoter for the murine CBFalpha2 gene: distinct roles and regulation in natural killer and T cell development. Dev Biol 229:363–382. https://doi.org/10.1006/dbio.2000.9991.
48. Bae SC, Ogawa E, Maruyama M, Oka H, Satake M, Shigesada K, Jenkins NA, Gilbert DJ, Copeland NG, Ito Y. 1994. PEBP2 alpha B/mouse AML1 consists of multiple isoforms that possess differential transactivation potentials. Mol Cell Biol 14:3242–3252. https://doi.org/10.1128/MCB.14.5.3242.
49. Ito Y. 2008. RUNX genes in development and cancer: regulation of viral gene expression and the discovery of RUNX family genes. Adv Cancer Res 99:33–76. https://doi.org/10.1016/S0065-230X(07)99002-8.
50. Durst KL, Hiebert SW. 2004. Role of RUNX family members in transcriptional repression and gene silencing. Oncogene 23:4220–4224. https://doi.org/10.1038/sj.onc.1207122.
51. Speck NA, Gilliland DG. 2002. Core-binding factors in haematopoiesis and leukaemia. Nat Rev Cancer 2:502–513. https://doi.org/10.1038/nrc840.
52. Takahashi A, Satake M, Yamaguchi-Iwai Y, Bae SC, Lu J, Maruyama M, Zhang YW, Oka H, Arai N, Arai K. 1995. Positive and negative regulation of granulocyte-macrophage colony-stimulating factor promoter activity by AML1-related transcription factor, PEBP2. Blood 86:607–616.
53. Behrens K, Triviai I, Schwieger M, Tekin N, Alawi M, Spohn M, Indenbirken D, Ziegler M, Müller U, Alexander WS, Stocking C. 2016. Runx1 downregulates stem cell and megakaryocytic transcription programs that support niche interactions. Blood 127:3369–3381. https://doi.org/10.1182/blood-2015-09-668129.
54. Chen MJ, Yokomizo T, Zeigler BM, Dzierzak E, Speck NA. 2009. Runx1 is required for the endothelial to haematopoietic cell transition but not thereafter. Nature 457:887–891. https://doi.org/10.1038/nature07619.
55. Growney JD, Shigematsu H, Li Z, Lee BH, Adelsperger J, Rowan R, Curley DP, Kutok JL, Akashi K, Williams IR, Speck NA, Gilliland DG. 2005. Loss of Runx1 perturbs adult hematopoiesis and is associated with a myeloproliferative phenotype. Blood 106:494–504. https://doi.org/10.1182/blood-2004-08-3280.
56. Socolovsky M. 2007. Molecular insights into stress erythropoiesis. Curr Opin Hematol 14:215–224. https://doi.org/10.1097/MOH.0b013e3280de2bf1.
57. Socolovsky M, Murrell M, Liu Y, Pop R, Porpiglia E, Levchenko A. 2007. Negative autoregulation by FAS mediates robust fetal erythropoiesis. PLoS Biol 5:e252. https://doi.org/10.1371/journal.pbio.0050252.
58. Cai Z, de Bruijn M, Ma X, Dortland B, Luteijn T, Downing RJ, Dzierzak E. 2000. Haploinsufficiency of AML1 affects the temporal and spatial generation of hematopoietic stem cells in the mouse embryo. Immunity 13:423–431. https://doi.org/10.1016/S1074-7613(00)00042-X.
59. Mukouyama Y-S, Chiba N, Hara T, Okada H, Ito Y, Kanamaru R, Miyajima A, Satake M, Watanabe T. 2000. The AML1 transcription factor functions to develop and maintain hematogenic precursor cells in the embryonic aorta–gonad–mesonephros region. Dev Biol 220:27–36. https://doi.org/10.1006/dbio.2000.9617.
60. ENCODE Project Consortium, Kundaje A, Aldred SF, Collins PJ, Doyle F, Frietze S, Kaul R, Landt SG, Lee B-K, Rosenbloom KR, Sabo P, Shoresh N, Simon JM, Trinklein ND, Altshuler RC, Brown JB, Dong X, Dunham I, Ernst J, Hardison RC, Herrero J, Kelllis M, Kheradpour P, Lassman T, Lin X, Marinov GK, Mortazavi A, Parker SCJ, Schlesinger F, Thurman RE, Ward LD, Whitfield TW, Wilder SP, Wu W, Pazin MJ, Lowdon RF, Dillon LAL, Adams LB, Kelly CJ, Zhang J, Wexler JR, Good PJ, Feingold EA, Bernstein BE, Birney E, Crawford GE, Elinitski L, Gingeras TR, Green ED, Hubbard TJ, Kent WJ, Lieb JD, Myers RM, Starnatoyannopoulos JA, Tennebaum SA, Wold B, Khatun J, Yu Y, Wrobel J, Gunawardena HP, Kuiper HC, Maier CW, Xie L, Giddings MC, Epstein CB, Mikkelsen TS, Gillespie S, Goren A, Ram O, Zhang X, Wang L, Issner R, Coyne MJ, Durham T, Ku M, Truong T, Eaton ML, Kellis M, Djebali S, Davis CA, Merkel A, Dobin A, Lassmann T, Tanzer A, Lagarde J, Lin W, Xue C, Zaleski C, Rozowsky J, Röder M, Abdelhamid RF, Alioto T, Antoshechkin I, Baer MT, Batut P, Bell I, Bell K, Chakrabortty S, Chen X, Curado J, Derrien T, Drenkow J, Dumais E, Dumais J, Duttagupta R, Fastuca M, Fejes-Toth K, Ferreira P, Foissac S, Gao H, Gonzalez D, Gordon A, Howald C, Jha S, Johnson R, Kapranov P, Kingswood C, Li G, Park E, Preall JB, Presaud K, Ribeca P, Risk BA, Robyr D, Sammeth M, Sandu KS, Schaeffer L, See L-H, Skancke J, Suzuki AM, Takahashi H, Tilgner H, Trout D, Wang H, Hayashizaki Y, Harrow J, Hubbard TJ, et al. 2012. An integrated encyclopedia of DNA elements in the human genome. Nature 489:57–74. https://doi.org/10.1038/nature11247.
61. Cao W, Razanau A, Feng D, Lobo VG, Xie J. 2012. Control of alternative splicing by forskolin through hnRNP K during neuronal differentiation. Nucleic Acids Res 40:8059–8071. https://doi.org/10.1093/nar/gks504.
62. Xu J, Bauer DE, Kerenyi MA, Vo TD, Hou S, Hsu Y-J, Yao H, Trowbridge JJ, Mandel G, Orkin SH. 2013. Corepressor-dependent silencing of fetal hemoglobin expression by BCL11A. Proc Natl Acad Sci U S A 110:6518–6523. https://doi.org/10.1073/pnas.1303976110.
63. Kuvardina ON, Herglotz J, Kolodziej S, Kohrs N, Herkt S, Wojcik B, Oellerich T, Corso J, Behrens K, Kumar A, Hussong H, Urlaub H, Koch J, Serve H, Bonig H, Stocking C, Rieger MA, Lausen J. 2015. RUNX1 represses the erythroid gene expression program during megakaryocytic differentiation. Blood 125:3570–3579. https://doi.org/10.1182/blood-2014-11-610519.
64. Hu Z, Gu X, Baraoidan K, Ibanez V, Sharma A, Kadkol S, Munker R, Ackerman S, Nucifora G, Sauntharajah Y. 2011. RUNX1 regulates corepressor interactions of PU.1. Blood 117:6498–6508. https://doi.org/10.1182/blood-2010-10-312512.
65. Lutterbach B, Westendorf JJ, Linggi B, Isaac S, Seto E, Hiebert SW. 2000. A mechanism of repression by acute myeloid leukemia-1, the target of multiple chromosomal translocations in acute leukemia. J Biol Chem 275:651–656. https://doi.org/10.1074/jbc.275.1.651.
66. Hoogenkamp M, Lichtinger M, Krysinska H, Lancrin C, Clarke D, Williamson A, Mazzarella L, Ingram R, Jorgensen H, Fisher A, Tenen DG, Kouskoff

V, Lacaud G, Bonifer C. 2009. Early chromatin unfolding by RUNX1: a molecular explanation for differential requirements during specification versus maintenance of the hematopoietic gene expression program. Blood 114:299–309. https://doi.org/10.1182/blood-2008-11-191890.
67. Gravia A, Chondrou V, Kolliopoulou A, Kourakli A, John A, Symeonidis A, Ali BR, Sgourou A, Papachatzopoulou A, Katsila T, Patrinos GP. 2016. 21 October 2016. Correlation of SIN3A genomic variants with β-hemoglobinopathies disease severity and hydroxyurea treatment efficacy. Pharmacogenomics https://doi.org/10.2217/pgs-2016-0076.
68. Taniuchi I, Osato M, Egawa T, Sunshine MJ, Bae SC, Komori T, Ito Y, Littman DR. 2002. Differential requirements for Runx proteins in CD4 repression and epigenetic silencing during T lymphocyte development. Cell 111:621–633. https://doi.org/10.1016/S0092-8674(02)01111-X.
69. Voon DC-C, Hor YT, Ito Y. 2015. The RUNX complex: reaching beyond haematopoiesis into immunity. Immunology 146:523–536. https://doi.org/10.1111/imm.12535.
70. Kim WY, Sieweke M, Ogawa E, Wee HJ, Englmeier U, Graf T, Ito Y. 1999. Mutual activation of Ets-1 and AML1 DNA binding by direct interaction of their autoinhibitory domains. EMBO J 18:1609–1620. https://doi.org/10.1093/emboj/18.6.1609.
71. Vu LP, Perna F, Wang L, Voza F, Figueroa ME, Tempst P, Erdjument-Bromage H, Gao R, Chen S, Paietta E, Deblasio T, Melnick A, Liu Y, Zhao X, Nimer SD. 2013. PRMT4 blocks myeloid differentiation by assembling a methyl-RUNX1-dependent repressor complex. Cell Rep 5:1625–1638. https://doi.org/10.1016/j.celrep.2013.11.025.
72. Halevy T, Biancotti J-C, Yanuka O, Golan-Lev T, Benvenisty N. 2016. Molecular characterization of Down syndrome embryonic stem cells reveals a role for RUNX1 in neural differentiation. Stem Cell Rep 7:777–786. https://doi.org/10.1016/j.stemcr.2016.08.003.
73. Inoue K-I, Shiga T, Ito Y. 2008. Runx transcription factors in neuronal development. Neural Dev 3:20. https://doi.org/10.1186/1749-8104-3-20.
74. Yoshikawa M, Hirabayashi M, Ito R, Ozaki S, Aizawa S, Masuda T, Senzaki K, Shiga T. 2015. Contribution of the Runx1 transcription factor to axonal pathfinding and muscle innervation by hypoglossal motoneurons. Dev Neurobiol 75:1295–1314. https://doi.org/10.1002/dneu.22285.
75. Yoshikawa M, Masuda T, Kobayashi A, Senzaki K, Ozaki S, Aizawa S, Shiga T. 2016. Runx1 contributes to the functional switching of bone morphogenetic protein 4 (BMP4) from neurite outgrowth promoting to suppressing in dorsal root ganglion. Mol Cell Neurosci 72:114–122. https://doi.org/10.1016/j.mcn.2016.02.001.
76. Theriault FM, Nuthall HN, Dong Z, Lo R, Barnabe-Heider F, Miller FD, Stifani S. 2005. Role for Runx1 in the proliferation and neuronal differentiation of selected progenitor cells in the mammalian nervous system. J Neurosci 25:2050–2061. https://doi.org/10.1523/JNEUROSCI.5108-04.2005.
77. Chkheidze AN, Liebhaber SA. 2003. A novel set of nuclear localization signals determine distributions of the alphaCP RNA-binding proteins. Mol Cell Biol 23:8405–8415. https://doi.org/10.1128/MCB.23.23.8405-8415.2003.
78. Tang Y-S, Khan RA, Zhang Y, Xiao S, Wang M, Hansen DK, Jayaram HN, Antony AC. 2011. Incrimination of heterogeneous nuclear ribonucleoprotein E1 (hnRNP-E1) as a candidate sensor of physiological folate deficiency. J Biol Chem 286:39100–39115. https://doi.org/10.1074/jbc.M111.230938.
79. Chaudhury A, Hussey GS, Ray PS, Jin G, Fox PL, Howe PH. 2010. TGF-beta-mediated phosphorylation of hnRNP E1 induces EMT via transcript-selective translational induction of Dab2 and ILEI. Nat Cell Biol 12:286–293.
80. Dobin A, Davis CA, Schlesinger F, Drenkow J, Zaleski C, Jha S, Batut P, Chaisson M, Gingeras TR. 2013. STAR: ultrafast universal RNA-seq aligner. Bioinformatics 29:15–21. https://doi.org/10.1093/bioinformatics/bts635.
81. Ji X, Wan J, Vishnu M, Xing Y, Liebhaber SA. 2013. αCP poly(C) binding proteins act as global regulators of alternative polyadenylation. Mol Cell Biol 33:2560–2573. https://doi.org/10.1128/MCB.01380-12.
82. Ran FA, Hsu PD, Wright J, Agarwala V, Scott DA, Zhang F. 2013. Genome engineering using the CRISPR-Cas9 system. Nat Protoc 8:2281–2308. https://doi.org/10.1038/nprot.2013.143.
83. Doench JG, Fusi N, Sullender M, Hegde M, Vaimberg EW, Donovan KF, Smith I, Tothova Z, Wilen C, Orchard R, Virgin HW, Listgarten J, Root DE. 2016. Optimized sgRNA design to maximize activity and minimize off-target effects of CRISPR-Cas9. Nat Biotechnol 34:184–191. https://doi.org/10.1038/nbt.3437.
84. Love MI, Huber W, Anders S. 2014. Moderated estimation of fold change and dispersion for RNA-seq data with DESeq2. Genome Biol 15:550. https://doi.org/10.1186/s13059-014-0550-8.
85. Bodenhofer U, Bonatesta E, Horejš-Kainrath C, Hochreiter S. 2015. msa: an R package for multiple sequence alignment. Bioinformatics 31:3997–3999.